Master's Thesis

Dynamic Ringing Suppression in a CAN-FD transceiver using peak voltage detection and impedance switching

Dohoon Lee

Department of Electrical Engineering

Graduate School of UNIST

2020

Dynamic Ringing Suppression in a CAN-FD transceiver using peak voltage detection and impedance switching

Dohoon Lee

Department of Electrical Engineering

Graduate School of UNIST

Dynamic Ringing Suppression in a CAN-FD transceiver using peak voltage detection and impedance switching

A thesis
submitted to the Graduate school of UNIST
in partial fulfillment of the requirements for the degree of
requirement for the degree of
Master of Science

Dohoon Lee

6.14.2020
Approved by

Advisor
Prof. Myunghee Lee

Dynamic Ringing Suppression in a CAN-FD transceiver using peak voltage detection and impedance switching

Dohoon Lee

This certifies that the thesis of Dohoon Lee is approved.

6.14.2020

Advisor: Prof. Myunghee Lee

Prof. Franklin Bien

Prof. Jaejoon Kim

ABSTRACT

In the automotive system, CAN(Controller Area Network) is a communication protocol between controller and sensor, actuator. And, it is important to safety transmit and receive message through CAN bus line. Recently, As the number of connected controllers and provided sensor in the vehicle are increased, the demand for an improved network system delivering a higher speed and a large amount of data at a time is increasing. CAN FD(Flexible Data-Rate) is improved protocol of the original CAN. CAN FD is designed to increase the data transfer rate up to 5Mbps and has lager data size than classical CAN. However, high speed transceiver CAN FD is more critical to signal distortion. The signal distortion, called ringing, is caused by reflection and superposed signal due to the mismatch of dynamic parameters such as propagation delay. This distortion signal causes communication errors. So, it is need to consider a signal reflection and RF immunity in the bus interface to remove communication error. Previous ringing suppression circuit is using the state detection method operated with suppression action regardless of ringing situation and only depend on the recessive region of signal.

In this thesis, the new ringing suppressed method directly sensing the ringing voltage will be proposed to achieve high performance about ringing situation. This ringing suppression circuit is designed by using peak voltage detection and switch control to match resistance at CAN FD node. Peak detection circuit is sampling the ringing voltage and holding the peak of ringing voltage, then, comparator controls the impedance switch according to the magnitude of peak voltage. And, the CAN FD transceiver with ringing suppression circuit was fabricated using a 0.18μm automotive BCDMOS process. As result, this proposed circuit shows high RF immunity and better performance than previous ringing suppression method.

KEYWORD: Automotive IC, Controller Area Network with Flexible Data-rate, Transceiver, Reflection, Ringing

CONTENT

GLOSSARY

BCDMOS	Bipolar, CMOS and LDMOS
BGR	Band-gap Reference
CAN	Controller Area Network
CAN-FD	CAN with Flexible Data-rate
CM	Common-mode
ECU	Electronic Control Unit
EFT	Electrical Fast Transient
EM	Electromagnetic
EME	Electromagnetic Emission
EMI	Electromagnetic Immunity
ESI	Error Status Information
IC	Integrated Chip
IVN	In-vehicle Network
ISO	International Organization for Standardization
LDMOS	Lateral Diffused MOS
RF	Radio Frequency
RX	Receiver
RXD	Receive Data
SOA	Safe Operating Area
TRX	Transceiver
TSD	Thermal Shutdown
TX	Transmitter
TXD	Transmit Data

1. Introduction

In the Automotive industry, CAN is one of the most used in vehicle network system. Because, CAN has an advantage in terms of low cost and robustness. Recently, The number of ECUs(Electronic Control Units) is increased to support comport, safety function in vehicle. But, there are some limitation in CAN transceiver Spec. CAN is communication with each CAN up to 1Mbps and the size of message is restricted to 8byte. This spec can't satisfy the demand of more ECUs connected vehicle network. It is need to the expanded message frame and more higher speed transceiver in this network. To satisfy this demand, CAN with flexible data rate (CAN FD) was proposed by Robert Bosch[1].

In this introduction section, the background of CAN and CAN FD will be explained and this section focuses on the different point between CAN and CAN FD. After that, additional consideration for electromagnetic emission will be discussed due to the increased data ration in the CAN FD.

1.1 CAN and CAN-FD

Classical CAN is internationally standardized by the International Organization for Standardization (ISO 11898) [2]. The main characteristic of CAN signal is two differential signaling method through twist cable to achieve robust operation supporting a maximum data-rate of 1Mbps. Fig. 1.1 shows the waveforms of CANH and CANL of a CAN bus. Recently, CAN-FD has been introduced which has also been standardized by ISO. It supports higher data-rate, up to 5Mbit/s in ISO documents, and able to send a longer message than classical CAN. Some changes exist in CAN-FD frame formats. CAN-FD allows bit times for certain fields that are shorter than the classical CAN bit time [4]. By reducing the bit time, the number of data bytes of the data field increases to 64 bytes compared to 8 bytes in the classical CAN. Fig. 1.2 shows the difference of the frame format between CAN and CAN-FD.

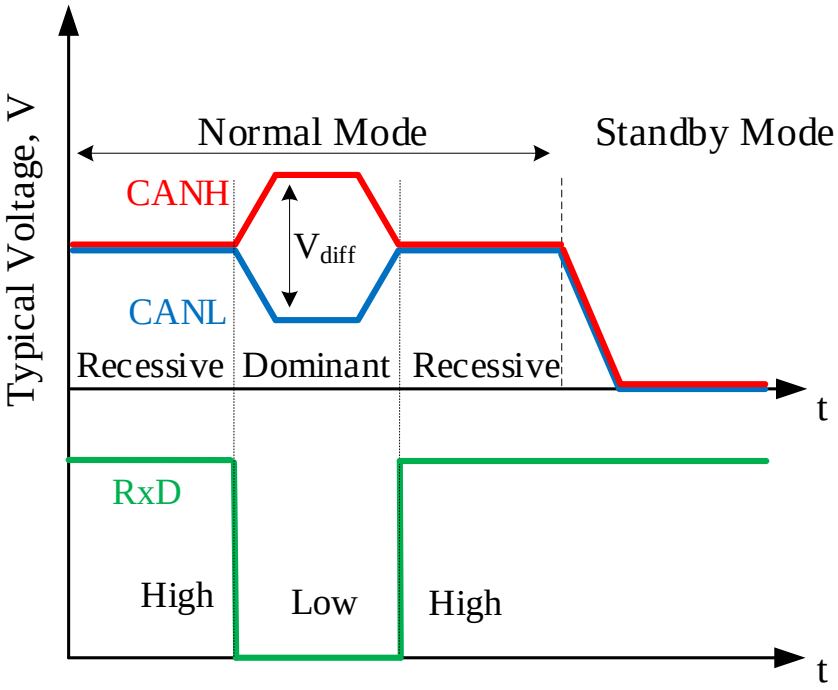

Fig. 1.1 A signal definition of the CAN protocol at CAN bus.

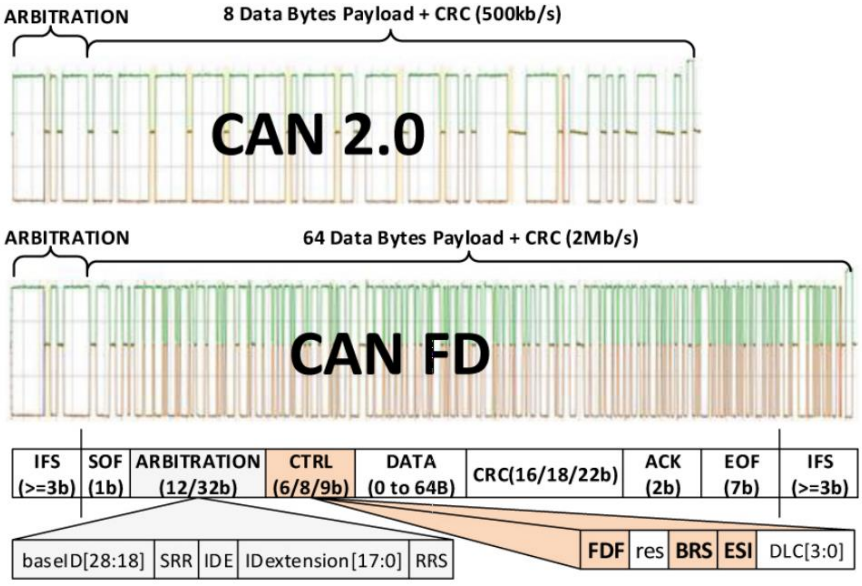

Fig. 1.2 Data frames compared with classical CAN and CAN-FD.

1.2 Safety Issue: EMI consideration form signal reflection

EMC issues have been one of the main reasons for redesigning automotive ICs. The automotive industry requires a high level of EMC. Achieving robustness against EMI and low EME is one of the most major challenges in designing a CAN-FD transceiver. The automotive communication networks such as classical CAN, CAN-FD and Local Interconnected Network (LIN) function as antennas which can emit and receive Radio Frequency (RF) disturbances. Using CAN-FD with a high data-rate, the fast transitions of the CAN bus signals generate high-frequency RF disturbances affecting other automotive ICs sensitive to EMI. The RF disturbances on the bus can also cause corrupting duty-cycle and change the logical state on the bus signals. These issues result in functional failures which are the most critical problem in the communication network. Designing a low EME CAN-FD transceiver, matching the CAN bus on switching behavior is the key factor in reducing EME and the cost of RF filters. But, RF filter has propagation delay to critical to the rate of CAN FD message communication.

To overcome these problems, this thesis shows added Ringing suppression block with matching characteristic impedance between node and cable, using Peak detection and holder circuit. The concept of ringing suppression is presented in Section 3.

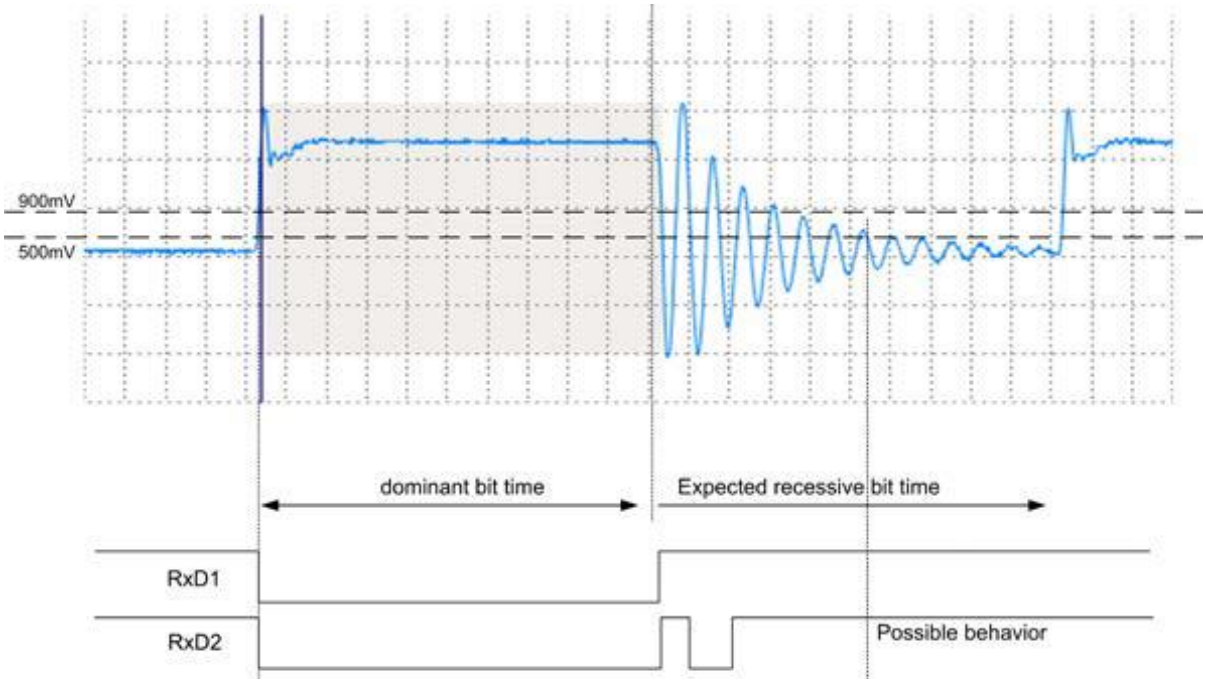

Fig. 1.3 Ringing CAN bus signal with receiver threshold voltage 500mV to 900mV

2. Design Considerations for CAN-FD Transceiver

2.1 Design Considerations for Automotive Environment

When designing the CAN-FD transceiver, the automotive environment should be considered. The automotive environment is a very harsh environment compared to the normal environment. It includes a wide range of temperatures and a variation in supply voltage, Electrical Fast Transient (EFT), mechanical and unwanted exposures. Also, the automotive transients must be considered according to ISO 7637 standard. For example, Load Dump, which causes transitions up to 40V, is an important consideration. Table 2.1 shows the hazards in the automotive environment. Some of these hazards, which include Temperature, voltages and electromagnetic impulses, are concerns when designing the automotive ICs. Fig. 2.1 shows the specification of an automotive battery.

Table 2.1 The hazards in the automotive environment.

Temperature	Driver interior	-40℃ to +85℃
	Underhood	-40℃ to +125℃
	On-engine	-40℃ to +150℃
	In the exhaust and combustion areas	-40℃ to +200-600℃
Mechanical Shock	During assembly (drop test)	3000g
	On the vehicle	50-500g
Mechanical Vibration		15g, 100Hz to 2kHz
Electromagnetic Impulses		100 to 200V/m
Exposure to	Common	Humidity, salt spray
	In some application	Fuel, oil, brake fluid, transmission fluid, ethylene glycol, exhaust gases

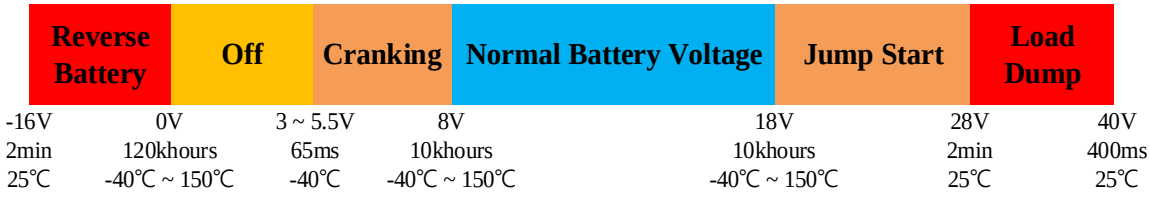

Fig. 2.1 Specification of automotive battery.

2.2 Specific Requirements for Classical CAN

Classical CAN has been introduced and widely used to communicate between microprocessors in an automotive system. In ISO 11898, there are specifications for the CAN physical layer which refer to the CAN transceiver. Table 2.2 shows the maximum rating of ports from ISO11898-5 which are one of the specifications for the CAN physical layer. The voltage ranges from -27V to 40V should be guaranteed at the CAN bus pins. This is because the CAN bus can be short-circuited to the supply lines even in the double battery and inverted double battery condition.

Table 2.2 Maximum ratings of CANH, CANL, and VSPLIT [2].

Nominal batter voltage (V)	Pin name	Voltage	
		Vmin	Vmax
14	VCAN_H	-27.0	+40.0
	VCAN_L	-27.0	+40.0
	VSplit	-27.0	+40.0

2.3 Specific Requirements for CAN-FD

The ISO standard of CAN-FD requires dynamic properties to cover higher bit rates than classic CAN. The specific properties should be met when designing a high bit-rate transceiver. The properties are listed below:

- Transceiver loop delay symmetry
- Transceiver transmitter (TX) delay symmetry
- Transceiver receiver (RX) delay symmetry

Table 2.3 shows the relationship between properties and parameters in ISO 11898-2 [2]. Table 2.4 to 2.6 shows the specific requirements of Loop delay symmetry, TX delay symmetry and RX delay symmetry.

Table 2.3 The relationship between properties and parameter in ISO 11898

Parameters in ISO	Link	Properties in CiA
Received recessive bit width $t_{Bit(RXD)}$	The minimal and maximal values of $t_{Bit(RXD)}$ => Calculate loop delay symmetry.	Loop delay symmetry
Transmitted recessive bit width $t_{Bit(Bus)}$	The minimal and maximal values of $t_{Bit(Bus)}$ => Calculate TX delay symmetry.	TX delay symmetry
Receiver timing symmetry Δt_{Rec}	Δt_{Rec} defines RX delay symmetry.	RX delay symmetry

Table 2.4 Loop delay symmetry characteristics.

Bit-rate (data phase)	Recessive $t_{Bit(RXD)}$ (min)	Recessive $t_{Bit(RXD)}$ (max)	t_{Bit} (nominal)	t_{Loop}	Load on the CAN bus	Load at RXD
1 Mbit/s	n.a.	n.a.	1000 ns	≤255 ns	60Ω‖100pF	15pF
2 Mbit/s	400 ns	550 ns	500 ns	≤255 ns	60Ω‖100pF	15pF
5 Mbit/s	120 ns	220 ns	200 ns	≤255 ns	60Ω‖100pF	15pF

Table 2.5 TX delay symmetry characteristics.

Bit-rate (data phase)	$t_{Bit(BUS)}$ (min)	$t_{Bit(BUS)}$ (max)	t_{Bit} (nominal)	Load on the CAN bus
1 Mbit/s	n.a.	n.a.	1000 ns	60Ω‖100pF
2 Mbit/s	435 ns	530 ns	500 ns	60Ω‖100pF
5 Mbit/s	155 ns	210 ns	200 ns	60Ω‖100pF

Table 2.6 RX delay symmetry characteristics.

Bit-rate (data phase)	Δt_{Rec} (min)	Δt_{Rec} (max)	t_{Bit} (nominal)
1 Mbit/s	n.a.	n.a.	1000 ns
2 Mbit/s	-65 ns	40 ns	500 ns
5 Mbit/s	-45 ns	15 ns	200 ns

2.4 Structure of CAN-FD Transceiver

The CAN-FD transceiver can be divided into two important parts: a transmitter and a receiver. The transmitter sends the signal to the CAN bus, converting a digital signal to an analog signal. The receiver performs the opposite operation, converting a bus differential signal into a digital signal.

A. Transmitter

Fig.2.2 is the most common structure of a transmitter which drives the CAN bus. The power stage consists of two pairs of Lateral Diffused MOS (LDMOS) operating as switches and diodes protecting supply rails from the reverse polarity voltage of bus pins. Two switches in the power stage operate in the triode region and are controlled by each driver block which turns the switches on and off. The switches are modeled on-resistances and the width of MOSFETs should be large. Reducing the on-resistances compared to the load, the CAN bus current is dependent on the load.

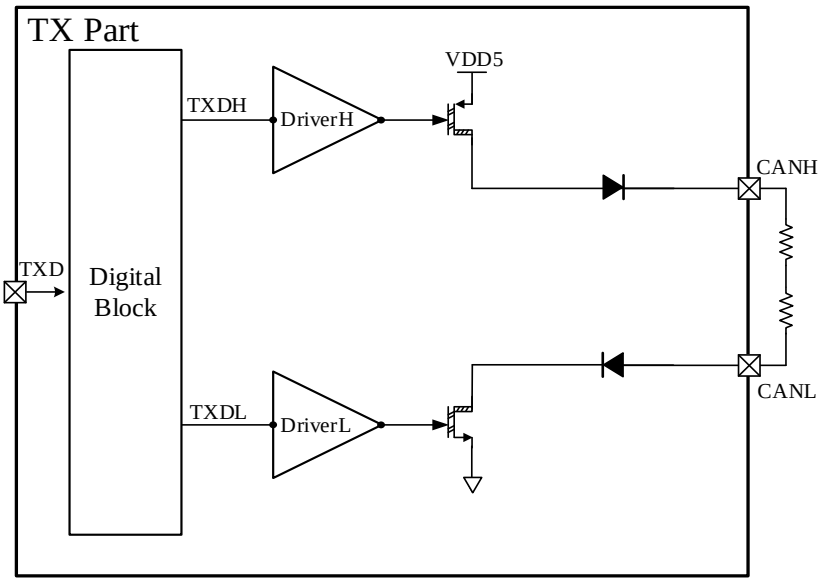

Fig. 2.2 Typical structure of CAN Tx

Fig. 2.3 shows the block diagram of the transmitter. Compared with the typical transmitter shown in Fig. 2.2, it consists of a Digital block, pre-driver (PD), power switch (PSW) and interface switch (IFSW). PSW and IFSW are included in the power stage which drives the CAN bus. Digital block converts TXD signal from MCU into TXDH and TXDL signals which can drive the high and low sides of power stage (PSW and IFSW) at the same time. PD consists of several unit blocks, called as PD, forming 16 cascade stages, and drives both sides of the power stage. PSW consists of 16 cascade stages of unit PSWs which can drive CANH and CANL to 2.06 mA. This structure achieves linear slopes of transitions at the CAN

bus. Each unit PSW acts as a current source, generating a constant current so as to achieve the symmetry of the CAN bus voltages. The objective of IFSW is to protect the transceiver from the reverse voltage on the CAN bus, which ranges from -27V to 40V. Outside of the chip, the equivalent resistors of terminal resistors of the CAN bus are represented as 60Ω.

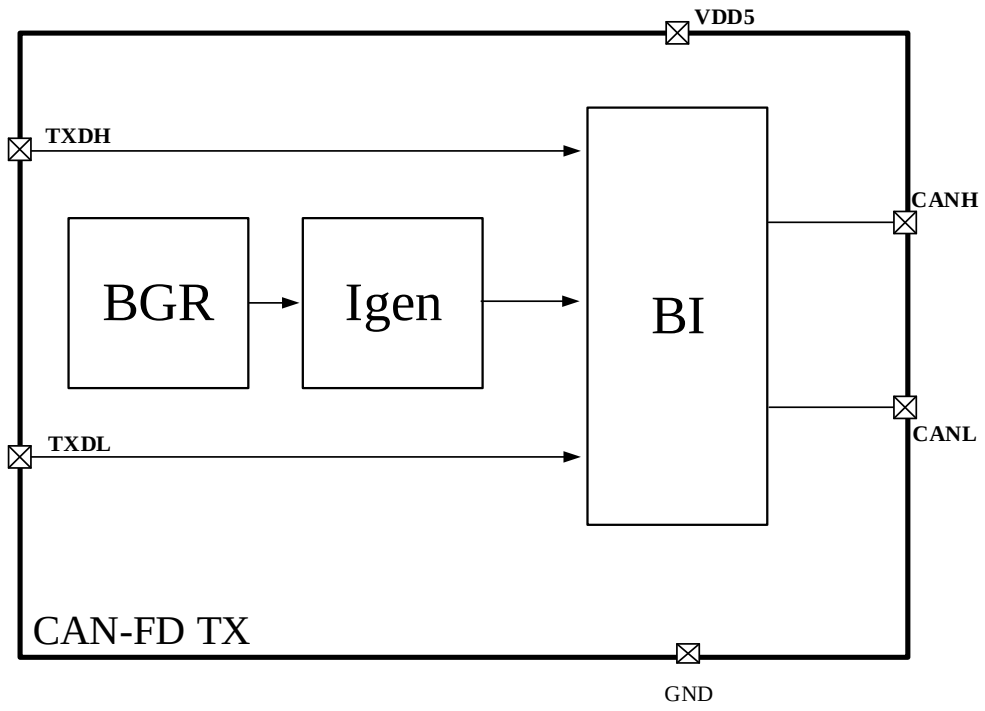

Fig. 2.3 Block diagram of CAN FD transmitter.

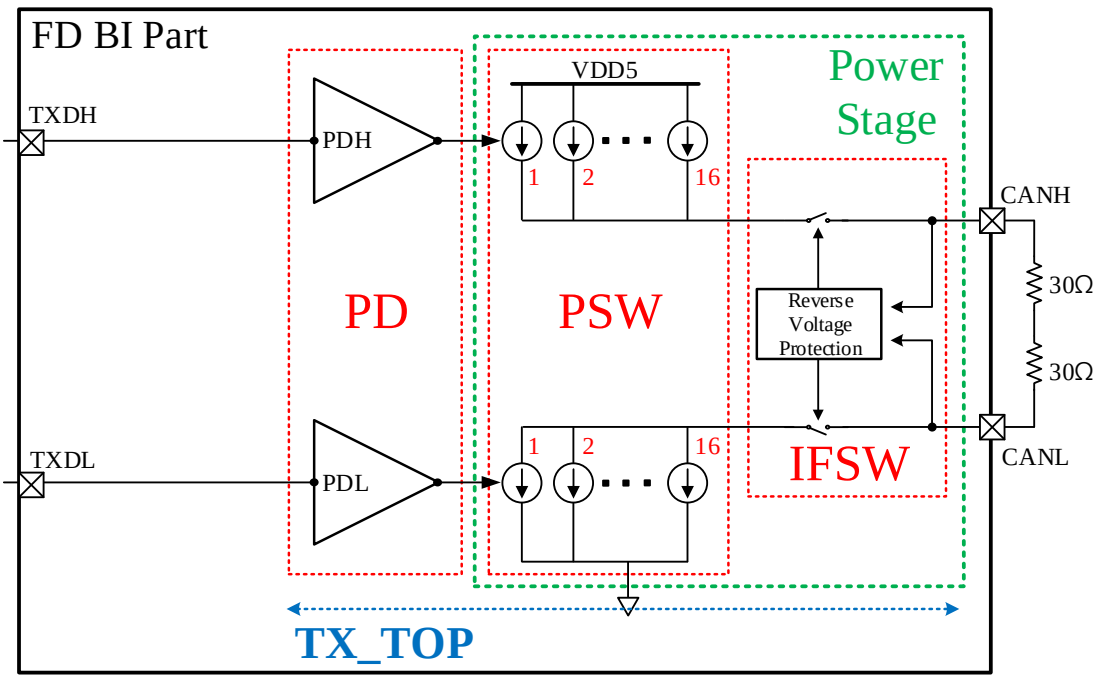

Fig. 2.4 Structure of Bus interface in CAN FD

B. Receiver

Fig 2.5 is one of the cases of receiver which receives CAN bus signal through the bus line. It is composed of Voltage divider and Offset block with Comparator. CANH and CANL signal are fed to differential receiver that senses the voltage difference and converts it into a logic signal RxD. The receiver is composed of three stages. First stage provides voltage divide function. The resistive divider brings CANH and CANL to low level voltage compatible with the circuits supplied by VDD. Then, Second stage is a differential common source degeneration amplifier making offset voltage to compare driving CANH and CANL. This offset voltage is adjusted by trimming current. RxComp is composed of differential amplifier and a hysteresis comparator. Noise at the CAN bus signal can cause output transition above and below the threshold voltage resulting in an erratic output signal. Thus, the hysteresis range should be wide enough to reject the noise from the CAN bus. It converts the CAN bus signal to the digital signal for the digital block of the CAN transceiver.

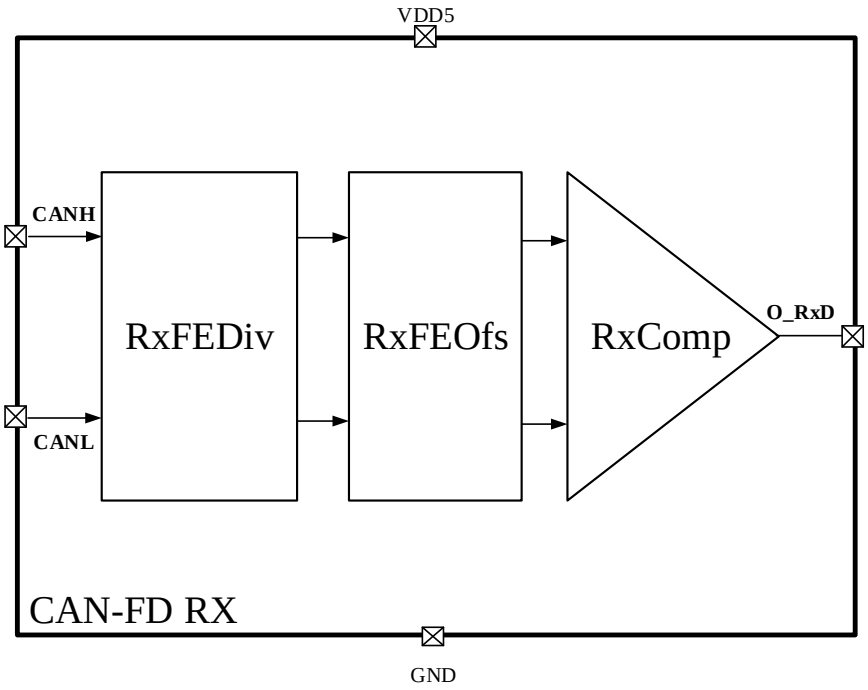

Fig. 2.5 Block diagram of CAN FD Receiver.

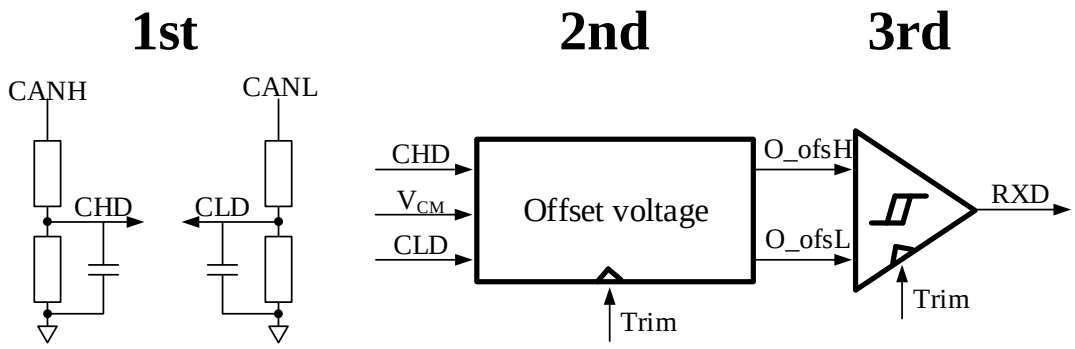

Fig. 2.6 Functional Stage of CAN FD Receiver.

3. Principle of Ringing suppression in CAN-FD

3.1 Concept of reflection in bus interface system

The CAN-FD transceiver need to achieve higher data rates under the conventional network size and the number of connected ECUs. In this case, there are some problem issues about EMI due to reflection through impedance mismatching. So, I propose ringing suppression circuit to prevent signal waveform from ringing voltage. According to CAN FD Spec, CAN FD data rate up to 5Mbps under the conventional network configuration and increase the ECUs connected to transceiver. More fast speed makes more critical about ringing in CAN communication system.

A. Operation of CAN node

CAN node consists of a CAN controller and a CAN transceiver. The CAN transceiver converts data signals into physical signals, and vice versa, to transfer the signals across a physical bus. Therefore, the driving and receiving features of a CAN transceiver affect the distortion of physical signals, ringing.
The part encircled by dotted lines in Fig. 3.1 is the interface section of a CAN transceiver to a physical bus line. In a dominant state, the output transistors Q1 and Q2 are turned on. Current flows through a physical bus and produces a nominal differential voltage of 2 V between the CAN-H and CAN-L lines. The impedance looking from the physical bus into the CAN transceiver becomes as low as several tens of ohms. In a recessive state, Q1 andQ2 are turned off and current is not delivered. A differential bus voltage is nominally driven toward 0 V. As only the receiver in the CAN transceiver is active, the impedance looking into the CAN transceiver becomes as high as several tens of kilo-ohms(= $Z_L >> Z_0$).

$\Gamma_L \equiv$ Load reflection coefficient

$$\Gamma_L = \frac{Z_L - Z_0}{Z_L + Z_0}$$

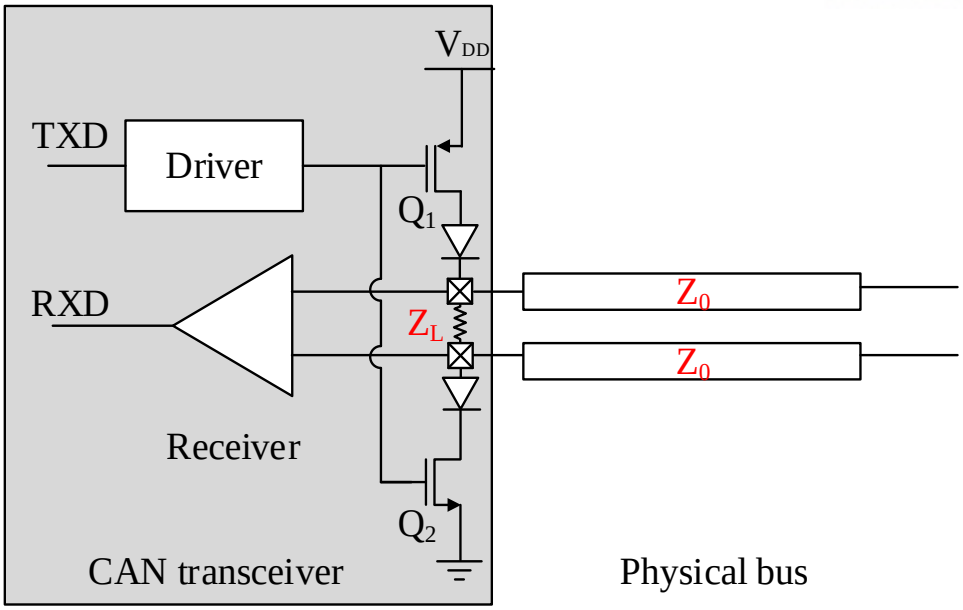

Fig. 3.1 Interface of CAN transceiver to physical bus.

B. Structure of a CAN FD bus system

In the linear topology recommended in the standards, the longest bus line, called the main bus, is terminated with two termination resistors at both ends, whose resistance is set to be the characteristic impedance of a bus line, Z_0(=120), for impedance match. Each CAN node is connected through relatively short lines, called stub lines, to a main bus, as shown in Fig. 3.2. This connection to the main bus is usually configured by a connector represented by the black circle and is called divergence point. In the star-like topology preferred by manufacturers because of its high productivity and low cost, more than two CAN nodes and more than two stub lines are connected to a divergence point, as shown in Fig. 3.3

The number of stub lines connected to each divergence point is n. Then, a linear topology is a specific case of n = 1. The impedance looking into the unterminated CAN node is Z_L. Looking into a divergence point from any CAN node, (n + 1) bus lines are shown in parallel, and their equivalent impedance is Z_T n+1. At the divergence point, the reflection and transmission coefficients Γ_d and T_d are given by

$$\Gamma_d = \frac{\frac{Z_T}{n+1} - Z_T}{\frac{Z_T}{n+1} + Z_T} = -n/(n+2)$$

$$T_d = 1 + \Gamma_d = 2/(n+2) \text{ (at the divergence point.)}$$

And, in front of the unterminated CAN node, the reflection and transmission coefficients Γ_L and T_L are given by

$$\Gamma_L = \frac{Z_L - Z_0}{Z_L + Z_0}$$

$$T_L = 1 + \Gamma_L$$

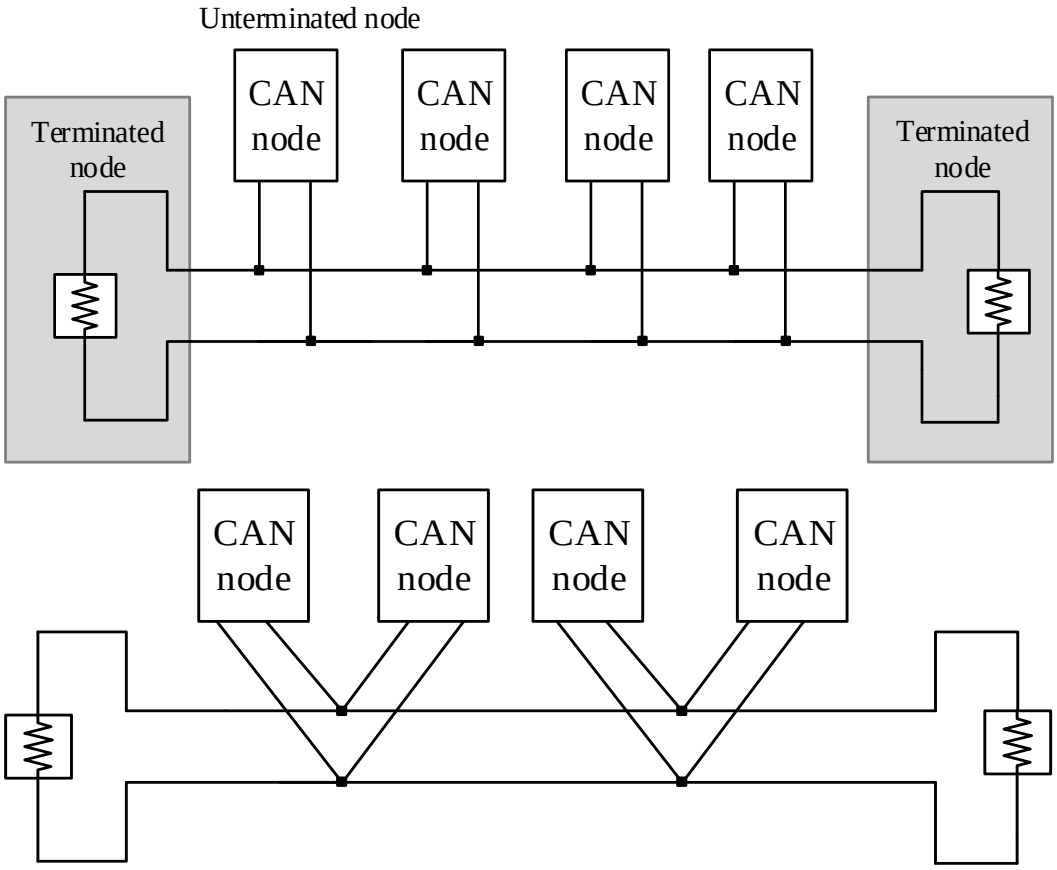

Fig. 3.2 CAN bus topologies: Recommended linear topology, star-like topology.

3.2 Quantitative analysis of Ringing in a CAN FD

The signal distortion on the physical bus in front of the transmitting unterminated CAN node in a dominant-to-recessive state transition was modeled and analyzed. This model is similar to terminated transmission line. So, We can analyze ringing by using transfer function.

A. Transfer function

The transfer function of the physical bus signal was modeled to estimate signal distortion and analyze the effects of the physical bus constituents. To isolate the effects of additional reflections at adjacent divergence points, it was assumed that there was only one divergence point on the main bus line.

Fig. 3.3 shows the simplified signal transmission and reflection at a divergence point. The number of unterminated CAN nodes connected to the connector is n, and consequently, (n + 2) CAN nodes are connected to one connector in total.

Tx and Rx in the boxes represent a transmitter and a receiver, respectively. Node #1, one of the

unterminated CAN nodes, acted as a transmitter and the others were in the receiver mode. Because the impedance of the terminated CAN node was matched with that of the bus line, its transmission and reflection coefficients were [1, 0], which means that the bus signal was not reflected at the terminated CAN node. In a recessive state, all unterminated nodes, including Node #1, had a high Z_L and identical reflection and transmission coefficients. From the equation, Vx(in) represents the differential voltage signal between the CAN-H and CAN-L terminals of each CAN node that propagated from the physical bus to the CAN node, and Vx(out) indicates that from the CAN node to the physical bus. When the reflection occurs only at CAN node, for $0 \le t < t_{trip}$, the transition signal ΔV is generation at t= 0. Considering $\Delta V = -2\ V_{dom}$, the signal at each unterminated CAN node is given by

For $0 \le t < t_{trip}, V_{1(in)}(k=0) = 0\ and\ V_{1(out)}(0) = \Delta V$

If n ≥ 2, $V_{2(in)}(0) = \cdots = V_{n(in)} = V_{in} = 0$

$$V_{2(out)}(0) = \cdots = V_{n(out)} = V_{out} = 0$$

➔ $V_{node1}(0) = V_{dom} + \Delta V$

Then, for $t_{trip} \le t < 2t_{trip}$, the reflected transition signal at the connector has returned

$$V_{1(in)}(k=1) = V_{1(out)}(0)e^{(-2al_s)} * \Gamma d + \sum_{i=2}^{n} V_{i(out)}(0)e^{(-2al_s)} * T_d$$

$$= V_{1(out)}(0)e^{(-2al_s)} * \Gamma d + (n-1)V_{out}(0)e^{(-2al_s)} * T_d$$

$$V_{1(out)}(1) = V_{1(in)}(1) * \Gamma_L$$

If $n \ge 2$, $V_{in}(1) = V_{out}(0)e^{(-2al_s)} * \Gamma_d + V_{1(out)}(0)e^{(-2al_s)} * T_d + \sum_{i=2}^{n} V_{i(out)}(0)e^{(-2al_s)} * T_d$

$$= V_{1(out)}(0)e^{(-2al_s)} * T_d + V_{out}(0)e^{(-2al_s)} * \Gamma_d + (n-2)V_{out}(0)e^{(-2al_s)} * T_d$$

$$V_{out}(1) = V_{in}(1) * \Gamma_L$$

➔ $V_{node1}(1) = V_{node1}(1) + V_{1(in)}(1) * T_L$

According to the result, generally, for k ≥ 2 and $k * t_{trip} \le t < (k+1)t_{trip}$

$$V_{in}(k) = V_{1(out)}(k-1)e^{(-2al_s)} * T_d + V_{out}(k-1)e^{(-2al_s)} * \Gamma_d + (n-2)V_{out}(0)e^{(-2al_s)} * T_d$$

$$V_{out}(k) = V_{in}(k) * \Gamma_L$$

➔ $V_{node1}(k) = V_{node1}(k-1) + V_{1(in)}(k) * T_L$

where α represents the attenuation constant of the bus line and exp(−2αls) represents the signal attenuation due to the resistance of the bus line.

Therefore, the effects of the length of a stub line, and the number of stub lines connected to connector, could be quantitatively analyzed by using transfer function.

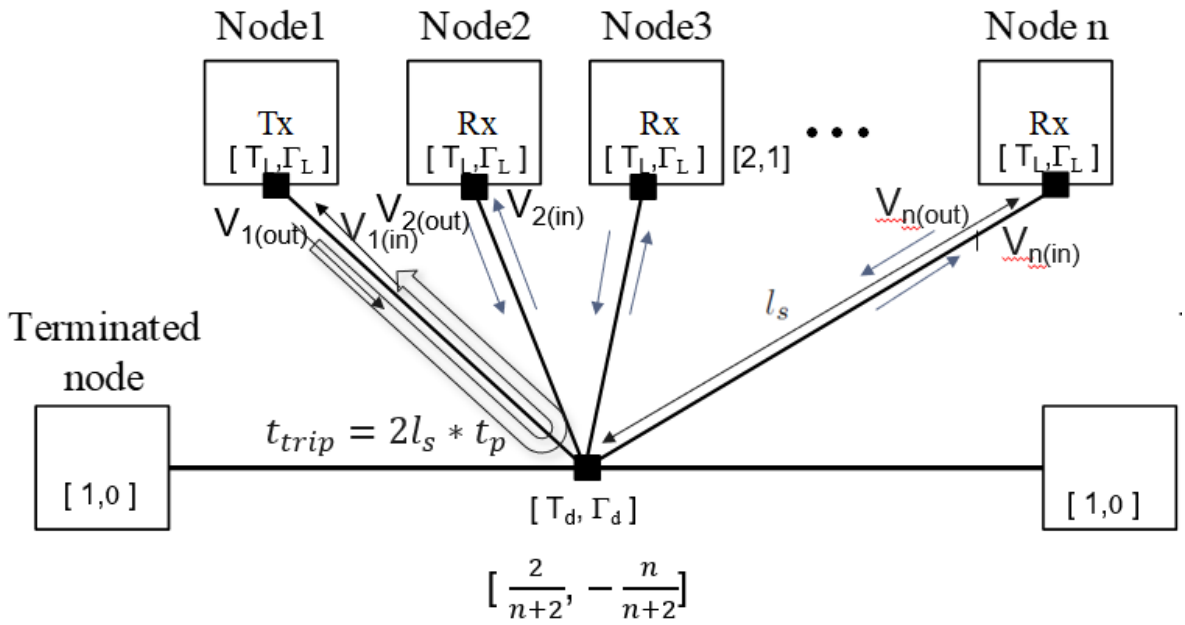

Fig. 3.3 Signal reflection and transmission.

B. Effects of cable length from transmitting CAN node to receiving node

Fig 3.4 shows the modeling of differential lengths of the stub line in a network configuration. It is shown that a longer round-trip delay, and the signal experiences a larger transition before the reflected signal at the divergence point return to the unterminated CAN node even though the transition.

$$T_{\text{delay}} \cong \frac{L}{\frac{c}{\sqrt{\varepsilon_r}}} \quad and \lambda = 2\,T_{delay}$$

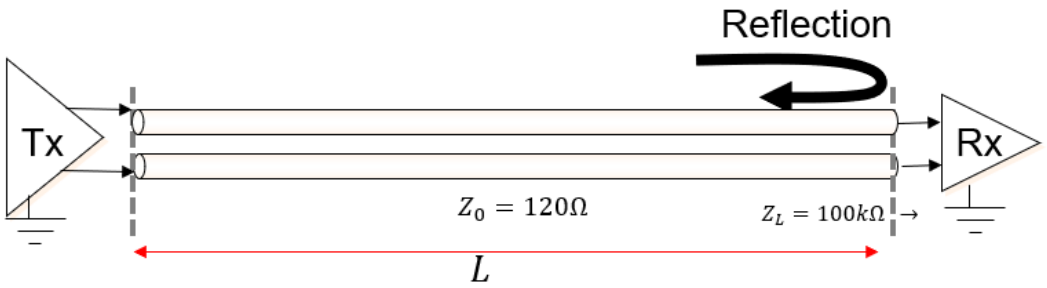

Fig. 3.4 Signal reflection and transmission.

C. Effect of the number of stub line connected to a joint connector

The effects of the number of stub lines connected to each connector were analyzed. According to simulation result, I set test environment for the number of connector n = 1, n = 2, n = 3, n = 4, n=5. The figure shows how to affect to CAN bus from each connector.

This result show that the magnitude of ringing increased with the number of stub line connected to a connector, because of the increase in the magnitude of Γ_d given by A) equations. Γ_d for n = 1,3,5 was $\Gamma_d = -\frac{1}{3}$, $-\frac{3}{5}$, $-\frac{5}{7}$. Respectively, A large Γ_d magnitude mean that a large portion of the transition signal was reflected at divergence point and returned to the unterminated CAN node, which created more intense ringing voltage. It is desirable that the number of stub lines connected to each connector is set to keep ringing less than 0.25 Vpp by considering the transition time and stub ling length.

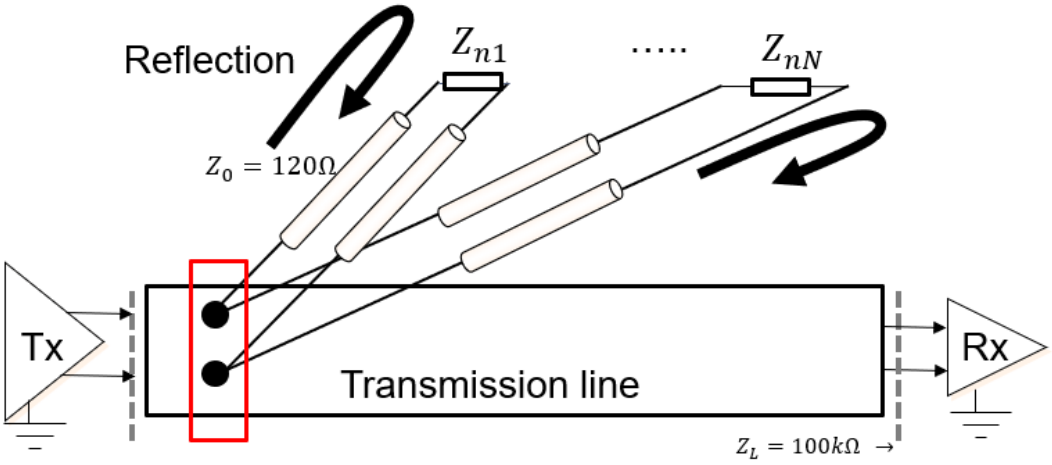

Fig. 3.5 Signal reflection and transmission.

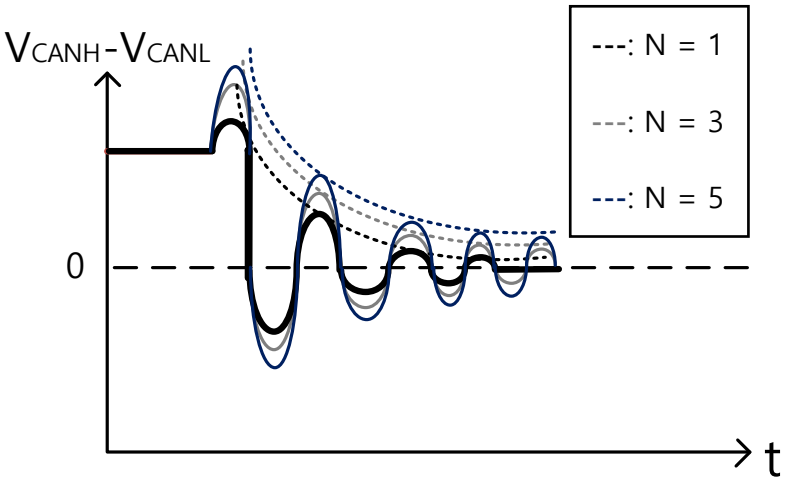

D. Analysis of effects of cable length and connector

A physical bus in a CAN-FD usually includes more than one connector and experiences additional distortion caused by reflections at neighboring connectors, as well as ringing caused by reflections at both ends of the stub lines analyzed in Section III. Therefore, the additional distortion was modeled and analyzed.

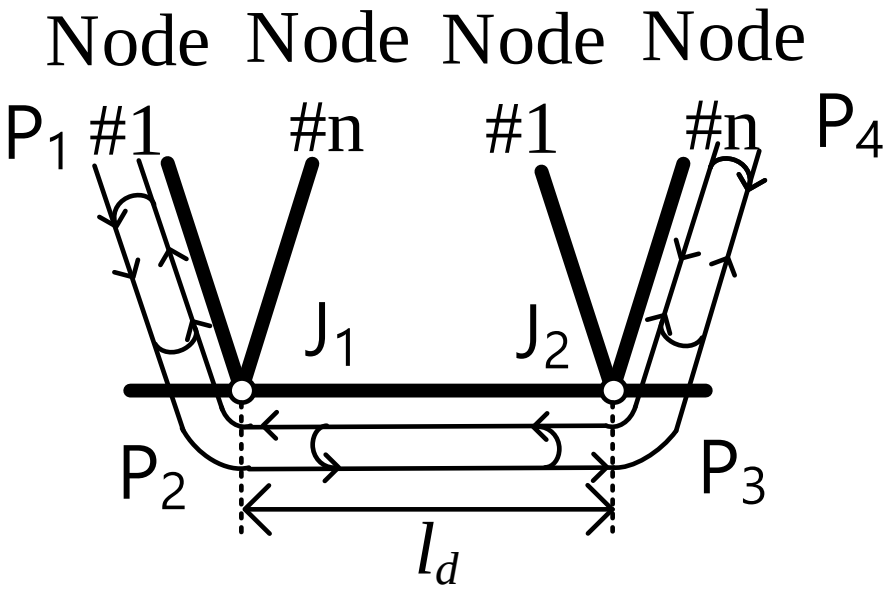

Figure 3.6. the model of CAN transmission line

Fig. 11 shows the simplified signal transmission and reflection in a physical bus including two connectors that are ld (m) apart. The thick line and thin solid arrow represent the physical bus line and signal flow, respectively. The gray circles, named J1 and J2, represent connectors and n unterminated CAN nodes are connected to each connector. This bus structure experiences reflection at four positions of P1, P2, P3, and P4, which are two connectors and the inputs of the unterminated CAN nodes connected to the two connectors. Let us assume that Node #1 connected to J1 transmits the signal. The signal is partly reflected at P2, which produces through P2 is reflected at P3, returns to P2, and undergoes partial reflection and transmission. Part of the signal transmitted through P3 is reflected at P4, returns to P3, and undergoes partial reflection and transmission. Part of each signal that returns to P2 is transmitted through P2 to Node #1 and superposed on the ringing.

The first return signals V1(in)(P3) and V1(in)(P4) to Node #1, which are reflected at P3 and P4, respectively, are described by

$$t \geq 2(ls + ld) * tp : V1(in)(P3)$$

$$= \mathrm{V1(out)}\ T_d \Gamma_d T_d * \exp(-2\alpha(ls+ld))$$

$$t \geq 2(ls + ld) * tp : V1(in)(P4)$$

$$= \mathrm{nV1(out)}\ T_d T_d\ \Gamma_d T_d T_d * \exp(-2\alpha(ls+ld))$$

After reflection at P_3, or P_4, the signal traveling to Node #1 undergoes additional. The return signal reflected at P3,P2 and P3 is

$$t \geq 2(ls + 2ld) * tp : V1(in)(P323)$$
$$= \text{V1(out)}\ T_d\Gamma_d\Gamma_d\Gamma_d T_d * \exp(-2\alpha(\text{ls}+2\text{ld}))$$

The first return signal reflected at P4,P3, and P4 is described by

$$t \geq 2(3ls + ld) * tp : V1(in)(P434)$$
$$= \text{V1(out)}\ \ T_d T_d \Gamma_s T_d(\Gamma_d\Gamma_s + (n+1)\Gamma_s T_d) T_d * \exp(-2\alpha(3\text{ls}+\text{ld}))$$

The first return signal reflected at P4,P2, and P3 is described by

$$t \geq 2(2ls + 2ld) * tp : V1(in)(P423)$$
$$= \text{V1(out)}\ \ T_d T_d \Gamma_s T_d \Gamma_s T_d * \exp(-2\alpha(\text{ls}+\text{ld}))$$

The first return signal reflected at P3,P2, and P4 is described by

$$t \geq 2(2ls + 2ld) * tp : V1(in)(P324)$$
$$= \text{nV}_{1(\text{out})}\ T_d\Gamma_d\Gamma_d T_d\ \Gamma_s T_d\ T_d * \exp(-2\alpha(\text{ls}+\text{ld}))$$

These return signals are partly transmitted to Node #1 and partly reflected. The signals reflected at Node #1 travel through the physical bus and repeat the partial transmission and reflection at P2, P3, and P4. The signal reflected at P2 undergoes the attenuation of $(\Gamma_d\Gamma_S + (n-1)\Gamma_S T_d)\exp(-2\alpha ls)$.

According to upper equation, the return signals are attenuation of V1(out) by multiplication of transmission and reflection coefficients at connectors and unterminated CAN nodes. The arrival time of each return signal depends on the lengths of stub lines and the distance between two connectors. Therefore, the physical bus signal is the superposition of ringing with its attenuated and delayed signals.

3.3 Proposed suppression method

The operation principle of ringing in physical is reflection and superposed signal due to the mismatch of dynamic parameters such as propagation delay and characteristic impedance of twisted wire, parasitic capacitive. And the ringing voltage cause overshoot voltage that is critical to message interpretation for recessive region. So, in order to suppression that's ringing, the ringing suppression method has to sense recession region of CAN bus signal and control load impedance to match dynamic parameter. Previous ringing suppression method is state change detection method that detect the edge of dominant to recessive state. However, there are some problem about data rate issues in this method.

In this paper, I will introduce peak detecting and holding method to sense the overshoot voltage and control the switch concerned in matching resistance.

A) State change detection circuit

In general, CAN in automation (CIA) proposed the state change detection method to sense the ringing. Fig. 12 shows the RSC (Ringing suppression circuitry) with state change detection can be implemented in the CAN transceiver. This circuit comprises the stat change detection circuit for detecting a change from dominant to recessive state, switch controller and the differential internal resistance R_{RSC}. When a dominant to recessive state change occurs on the CAN-H and CAN-L, the RSC adds the R_{RSC} to parallel connection about load impedance. After some certain suppression period, the R_{RSC} is switched-off again.

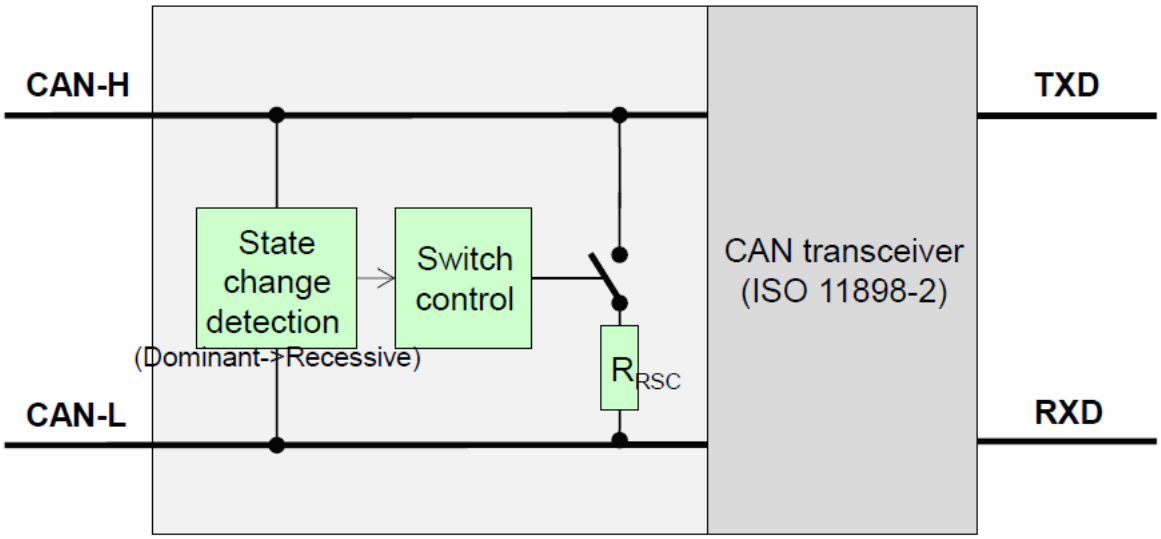

Figure 12. The Structure of RSC with state change detection method

The most important thing is the suppression duration time. The ringing suppression duration depends on the bit-rate. The duration of the function shall be within a minimum value of t_{bits} - t_{slope} . the $t_{Bit(Bus)}$ is defined in ISO 11898 as duration from the point when V_{diff} decreases under 500mV to the point when V_{diff} increases to 900mV. And, ts_{lope} is the duration of transition from recessive to dominant state. The max t_{slope} value is given by the actual slew rate that is defined as 5% of the $t_{Bit(TxD)}$ in ISO-11898. t_{RSC_START} is defined as the time from the point when decreasing V_{diff} reaches 500 mV to the start point of the RSC function. Then, t_{RSC_END} follows that's equation $t_{RSC\_END} + t_{Slope} \leq Min\,(t_{Bit(Bus)})$. About bit rate of 2Mbps, the table and ringing suppression timing can be expressed by using specified $t_{Bit(Bus)}$ in ISO-11898-2.

Table 3.1. Ringing suppression timing parameter for bit rate of 2Mbps.

Parameter	Minimum value	Maximum value	Remark
t_{RSC_START}	0 ns	50 ns	$t_{slope} \leq t_{Bit(TxD)}$*0.05
t_{RSC_END}	200 ns	410 ns	t_{Slope} = 25 ns Min ($t_{Bit(Bus)}$) = 435 ns

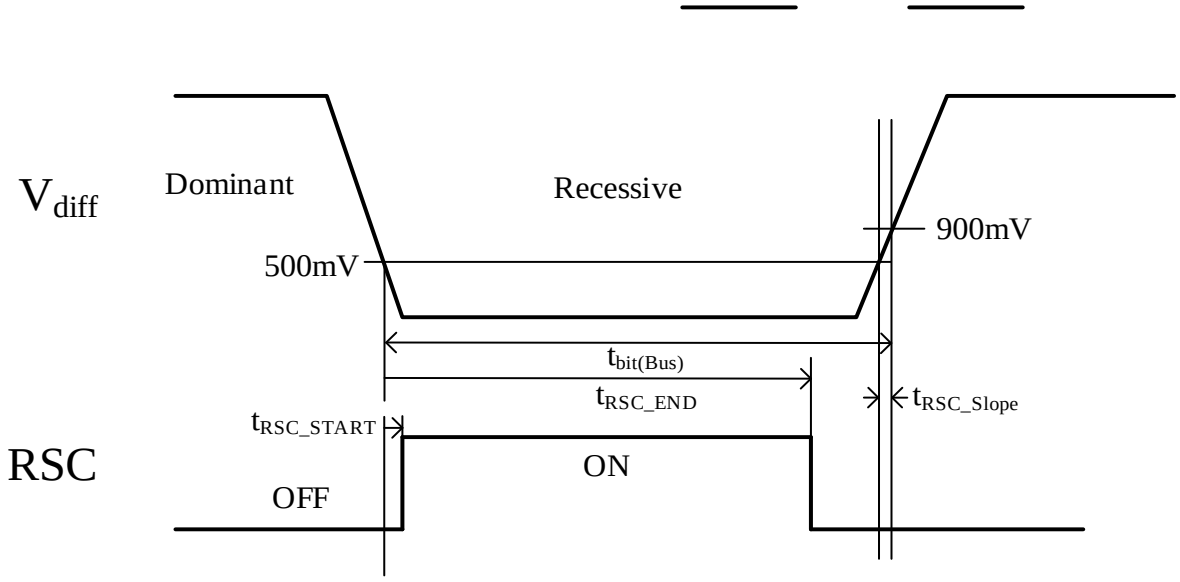

Figure 3.7. Ringing suppression timing for data -phase bit rate of 2Mbps

B) Improved ringing suppression method

There are some predictable problems about the sate change detection method. First, The RSC block always works regardless of whether a ringing occurs or not. It means the minimum RSC trigger threshold voltage is almost zero and the action of RSC is only depended on the edge between dominant and recessive state. This can cause synchronization errors, due to delayed dominant edge that can be delayed by capacitive load.

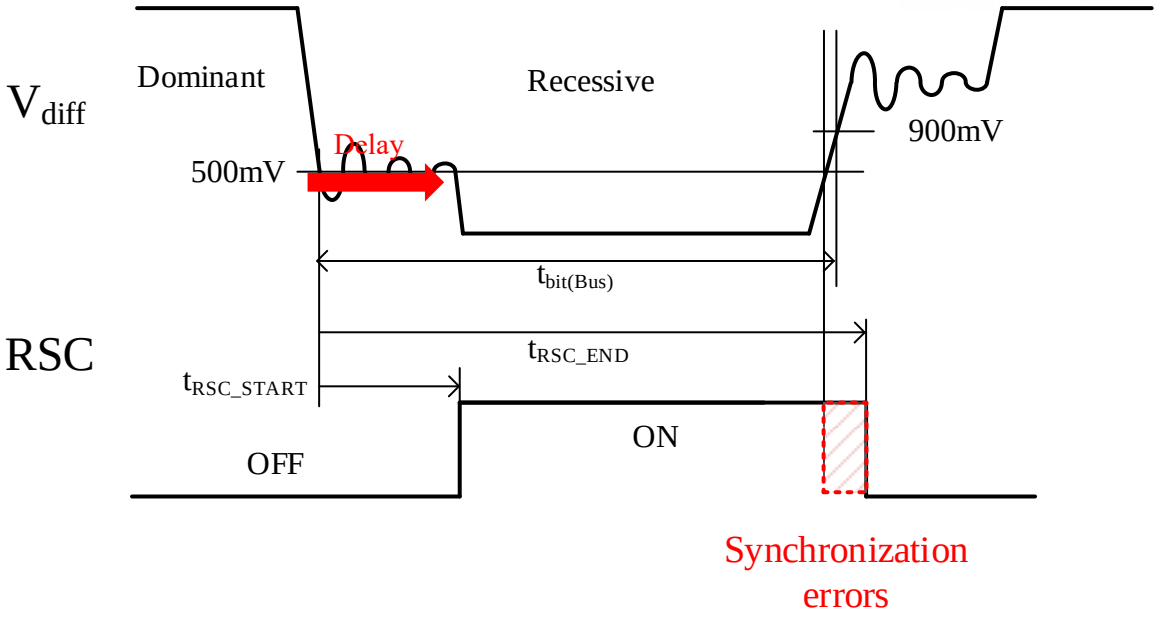

Figure 3.8. Ringing suppression timing for data -phase bit rate of 2Mbps with synchronization errors

Second, The other problem is this method is not proper solution about more high speed like 5Mbps. CAN FD support to up to 5Mbps and it is need to consider shorter period time per 1 bit. The higher the transmission rate has the narrower the time width of the bit. So, CAN FD with 5Mbps data rate has narrow wave length t_{bit} = 200ns. And, it is necessary to adjust a specific t_{RSC} and must control t_{RSC_END} according to data rate. However, RSC on delay ($t_{ON\ delay}$) is fixed that is set by RC time constant in state change detection circuit. And RSC must control t_{RSC_END} according to data rate. The Figure 3.9 show how to affect the message according to transceiver data rate. Although, They have same $t_{on\ delay}$, the width of bit time at 5Mbps is more critical affected by ringing suppression delay time. So, We need to reduce the start time of ringing suppression method.

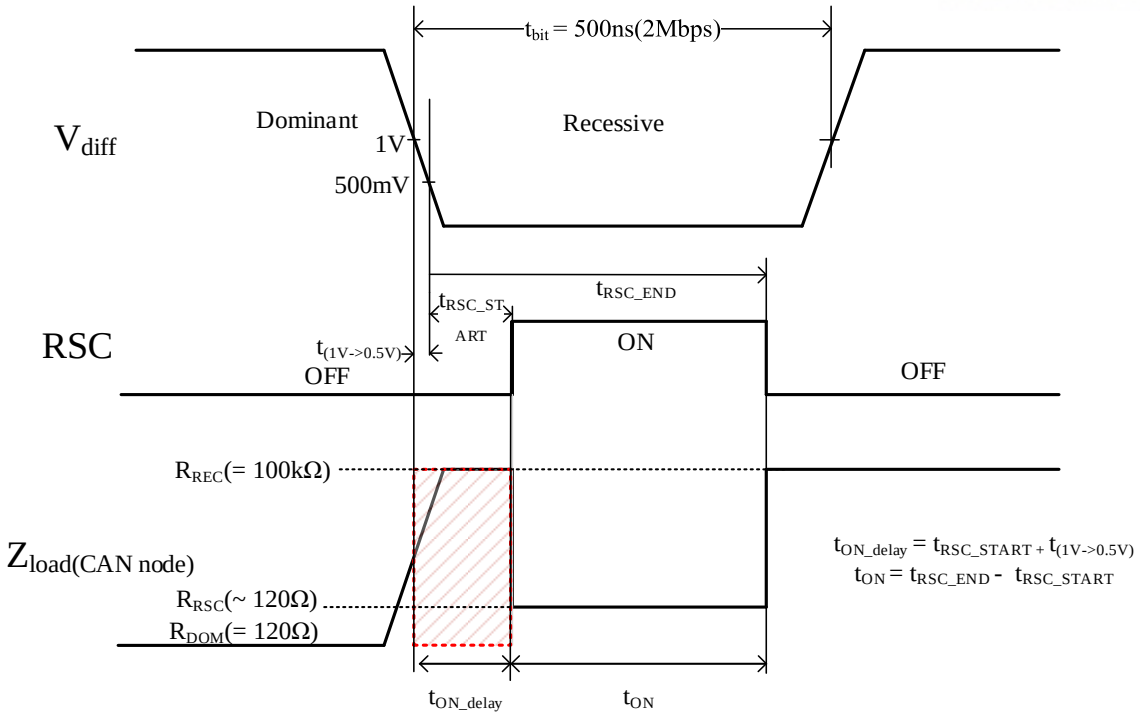

Figure 3.9.(a) Ringing suppression timing with wide ton delay at 2Mbps

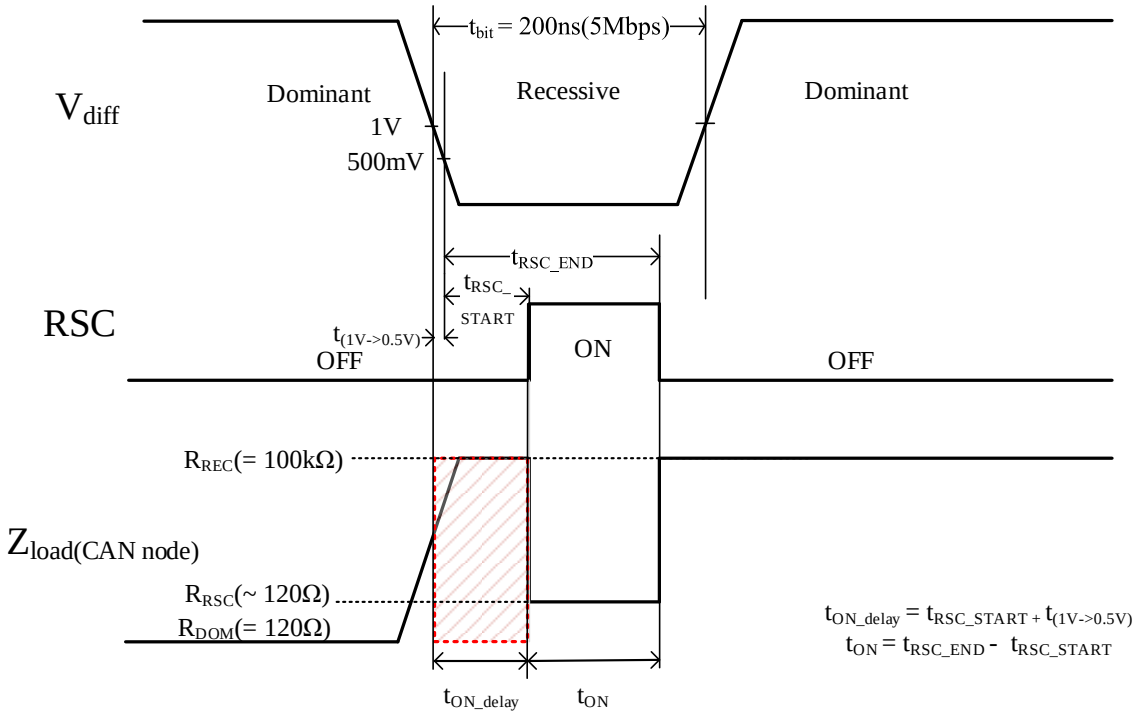

Figure 3.9.(b) Ringing suppression timing with wide ton delay at 5Mbps

3.4 Structure of Ringing suppression block

The CAN-FD transceiver need to achieve higher data rates under the conventional network size and the number of connected ECUs. In this case, there are some problem issues about EMI due to reflection through impedance mismatching. So, I propose ringing suppression circuit to prevent signal waveform from ringing voltage. According to CAN FD Spec, CAN FD data rate up to 5Mbps under the conventional network configuration and increase the ECUs connected to transceiver. More fast speed makes more critical about ringing in CAN communication system.

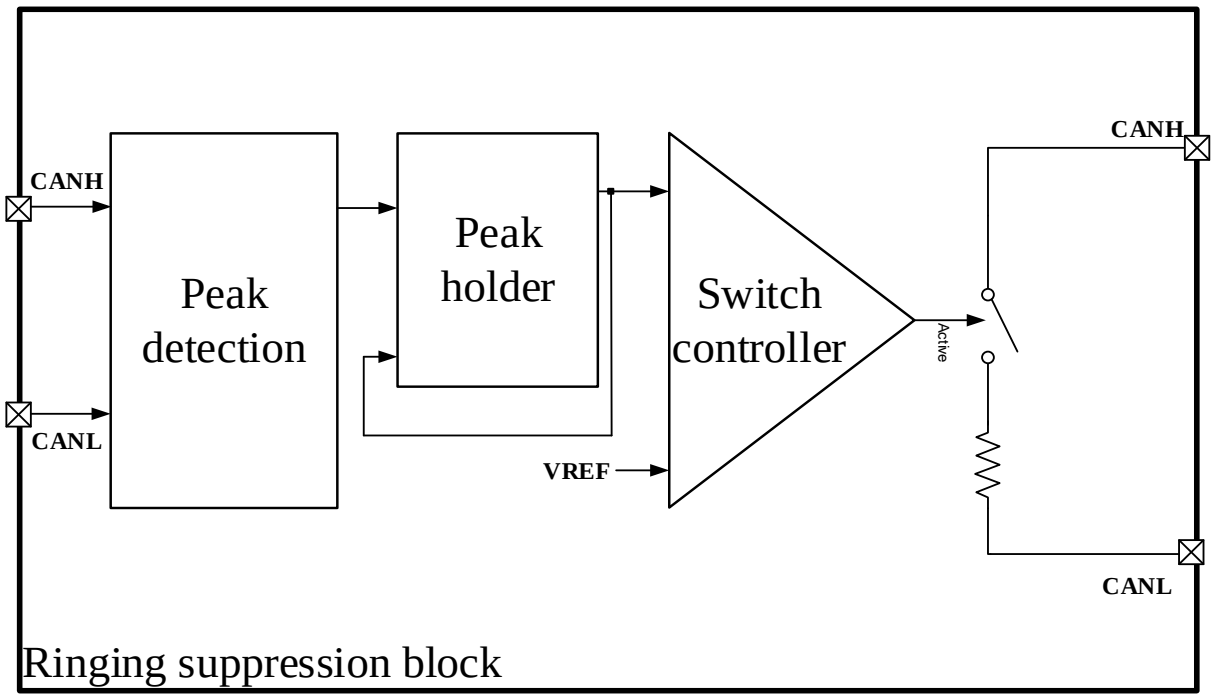

Fig. 3.10. Block diagram of ringing suppression block

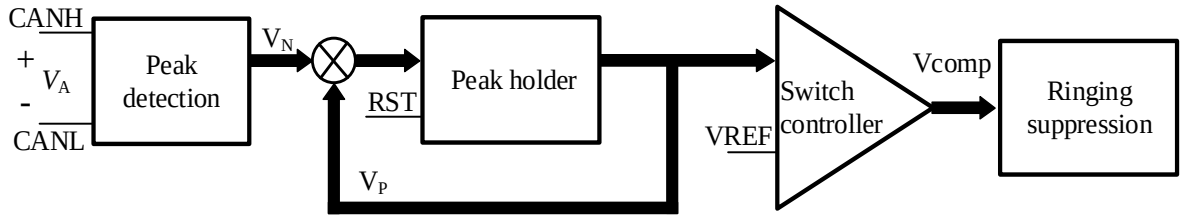

Fig. 3.11. the operation phase followed the ringing suppression by using peak detection and holder

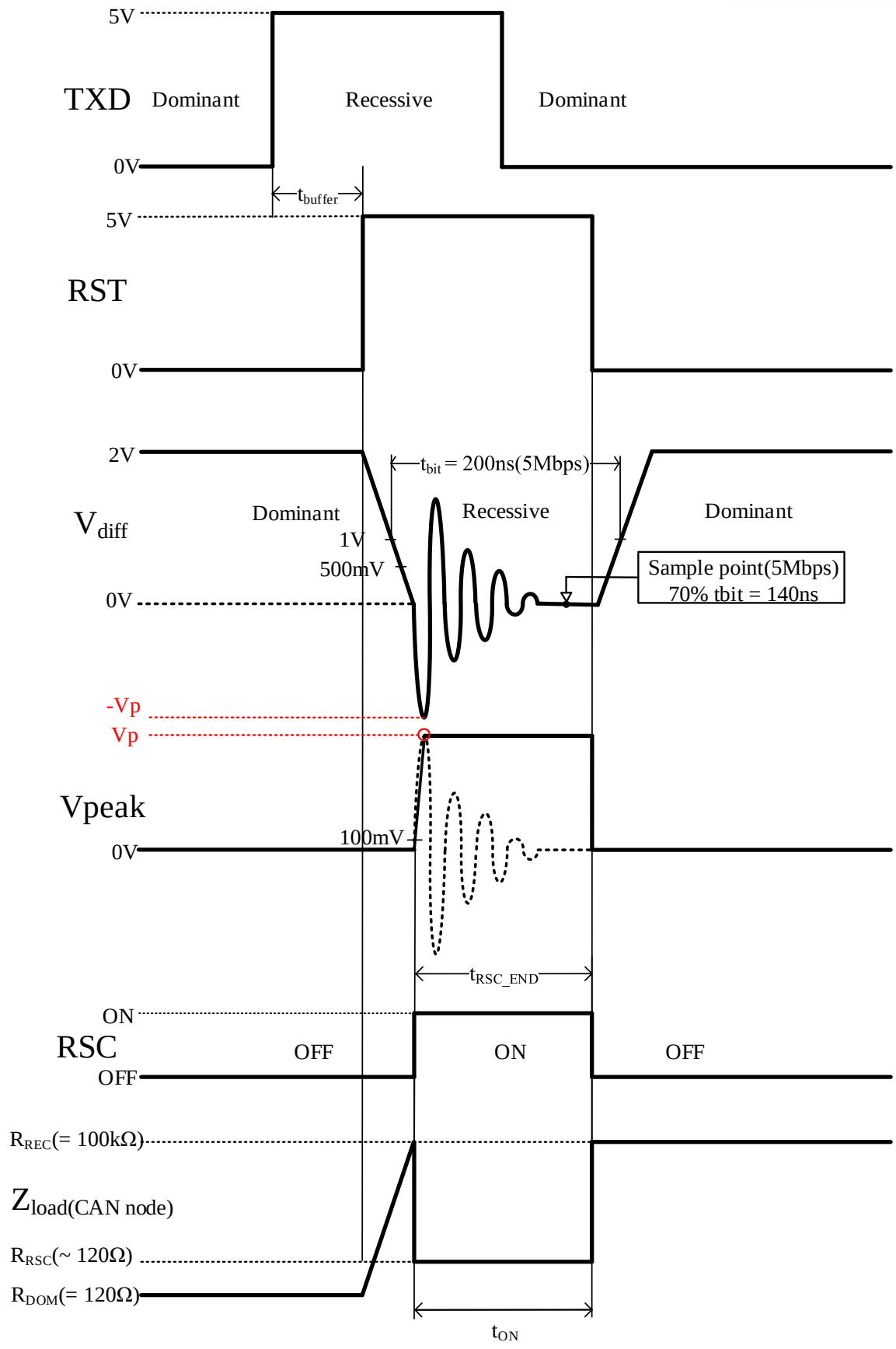

Fig. 3.12. the operation phase followed the ringing suppression by using peak detection and holder

3.5 Implementations of the Ringing Suppression Method

Ringing suppression block is composed of ringing detection circuit, peak holder and switch controller to turn on the matching resistance.

A. peak detection

the waveform of ringing voltage is similar to left half plane. Pole p2 is much farther away from fun. Can use smaller gm2, less power. LHP zero improves phase margin. Much faster op-amp with lower power and smaller C. Better slew rate as C_C is smaller.

$$V_{out} = -\frac{A_V(1+b_1 s)}{1+a_1 s+a_2 s^2+a_3 s^3}$$

$$z_1 = -\frac{1}{R_C C_C}$$

$$P_1 = \frac{1}{a_1} = -\frac{1}{g_{m2} R_2 R_1 C_C}$$

$$P_2 = -\frac{a_1}{a_2} = -\frac{g_{m2} R_1 C_C}{C_2(R_C C_C + R_1 C_C)} = -\frac{g_{m2} C_C}{C_L C_1}$$

$$P_3 = -\frac{a_2}{a_3} = -\left[\frac{1}{R_C C_C} + \frac{1}{R_1 C_1}\right]$$

$$f_{un} = \frac{[P_1]A_v}{2\pi} = \frac{g_{m1}}{2\pi C_C}$$

$$\rightarrow \quad H(s) = \frac{s+z1}{(s+p_1)(s+p_2)(s+p_3)}$$

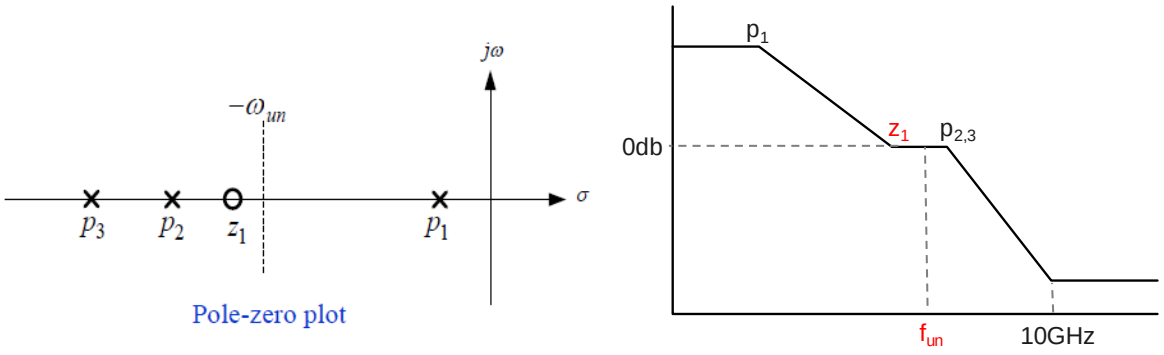

Considering down scaling in channel length L, more speed by using short length input mosfet.

$$f_{un} \propto \frac{V_{ov}}{L}$$

Then, Using compensation capacitance, Cc

$$f_{un} = \frac{2g_{m1}}{2\pi C_c}$$

$$z_1 \approx \frac{4g_{mn}}{3(C_c + C_A)} = \frac{4\sqrt{2}g_{mn}}{3(C_c + C_A)} \approx \frac{2\sqrt{2}}{3} w_{un}$$

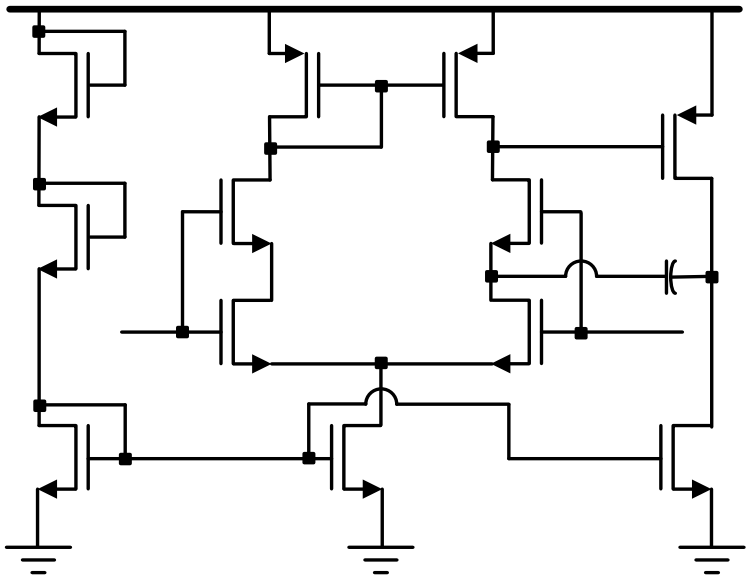

Figure.3.13. The circuit of peak detection op amp

B. Peak holder

The conventional peak hold circuit is shown in Fig 3. This circuit includes there phases including Reset, sample, holder function In the reset phase, the control signal “reset” is a high voltage level “1” to make the capacitance “C” discharged to ground voltage. In the sample phase, the control signal reset is a low voltage level “0”. When the input voltage Vin is larger than the output voltage Vout, the amplifier’s output is a low voltage level “0”, the PMOS with current mirror turns on and it charges the capacitance C until Vin is equal to Vout. When Vin is less than Vout, the amplifier’s output is “1” and that PMOS turns off. So, The output voltage Vout is so sustained as the maximum value of ringing voltage until the next reset signal given.

$$V_{out} = \frac{I_C * t_d}{C}$$

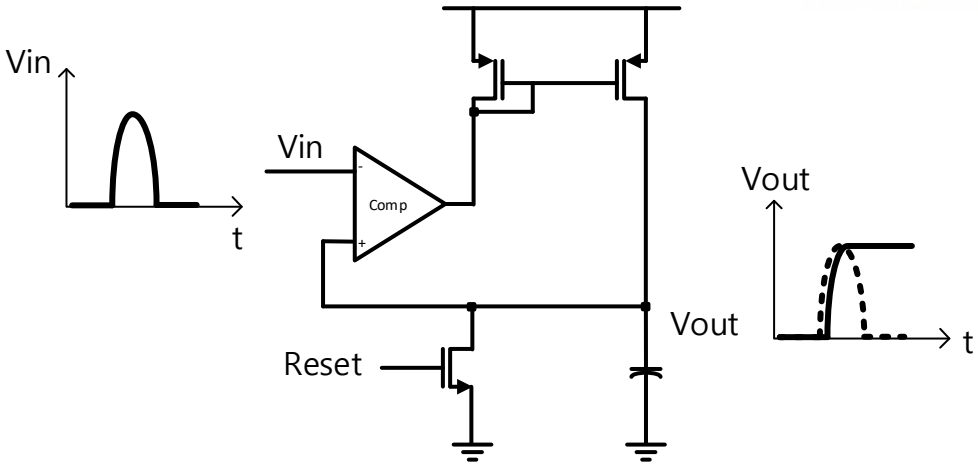

Fig. 3.14. Peak holder circuit

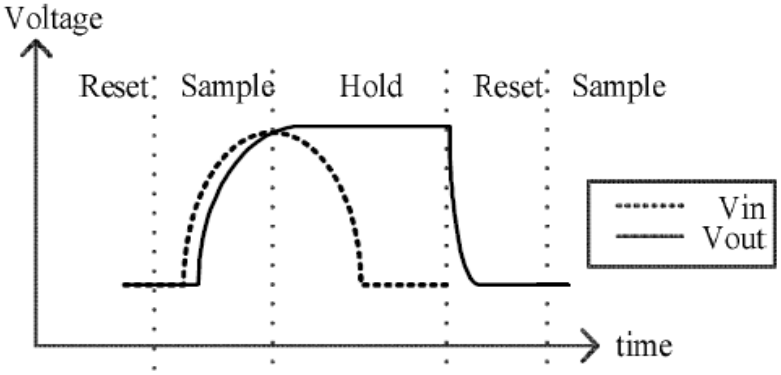

Fig. 3.15. Timing diagram of three phase(Reset, Sample, hold)

C. Switch controller

The function of Switch has input from hold peak voltage and the switch can be smaller resistance close to 120 for turn on when peak voltage is bigger than reference voltage. Setting V_{REF} is 100mV to quickly reaction to the ringing voltage sensing.

D. Ringing suppression

If the overshoot voltage is bigger than reference voltage, the switch MOSFET replaces received high resistance to Ron resistance. This Ron resistance suppressed overshoot voltage by using matching with cable characteristic resistance. In detail, Figure 3 shows a specific circuit implementation of the proposed method. The ringing suppression circuit is composed of four MOSs and a delay circuit. NMOS0 has the role to suppress the ringing and it is equivalent to the series circuit comprising a resistor and a switch described in Figure 5. The ON resistance of NMOS0 has a value that is almost equivalent to the characteristic impedance of the twisted pair cable. So, NMOS0 absorbs the incoming voltage wave of ringing frequency, which suppresses the ringing. The gate voltage is in the range between the voltages of the voltage source and CAN_L.

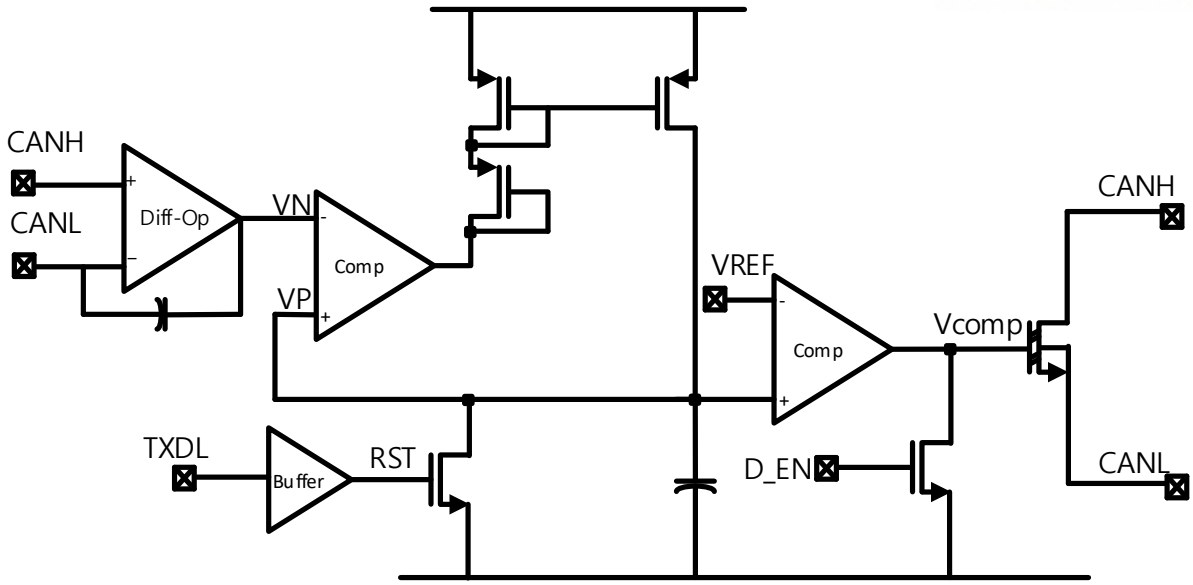

Fig. 3.16. The circuit structure of ringing suppression block

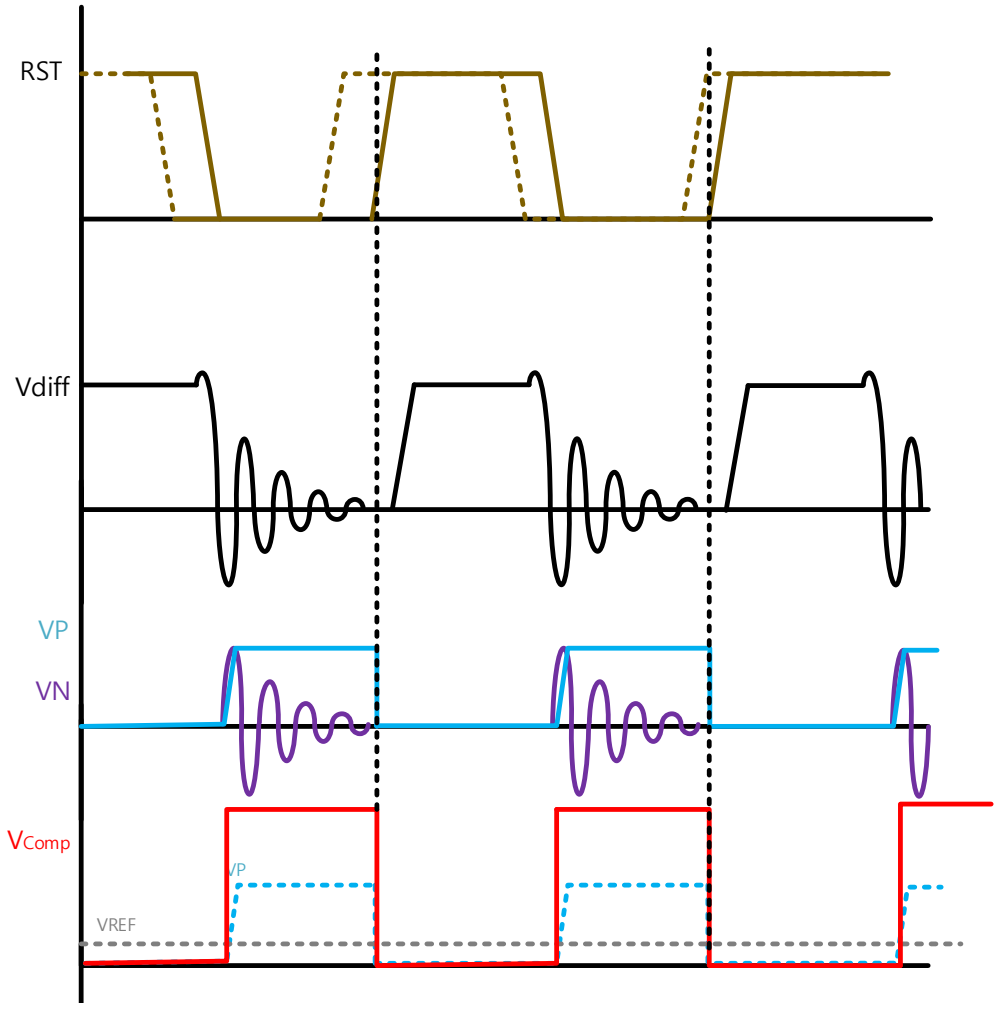

Figure 3.17. The waveform of operation of ringing suppression

3.6 Simulation result of proposed suppression method

A. Target experimental setup

Fig. shows the structure of a CAN bus for measuring ringing. The main bus line is 2 m long and terminated by 120-Ω resistors at both ends for impedance matching. At the middle of the main bus line, a connector is equipped for connecting stub lines. The test bus includes only one connector for clarity of ringing analysis. The unterminated CAN nodes with an additional 10-kΩ resistor are connected to the other end of the stub lines.

Fig. 7(b) shows a photograph of the fabricated CAN node consisting of a CAN transceiver, a linear regulator, an SMA connector, and a two-terminal connector. A Tx signal is input Fig. 7. (a) CAN bus test structure. (b) Photograph of the fabricated CAN node. into a transmitting CAN transceiver through an SMA connector on the left side of the node by a pulse generator (Agilent 33500B). Then, the transmitting CAN transceiver generates a physical bus signal that is transmitted to a bus line through the two-terminal connector on the right side of the node.

Node #1, connected to one of the stub lines, acted as a transmitter. When Node #1 changed its signal from a dominant state to a recessive state, a differential physical bus signal was measured at the transmitting Node #1, which corresponded to the worst ringing condition.

Measurements were performed by a differential probe (Keysight N2818A) with a bandwidth of 200 MHz and a digital oscilloscope (Keysight DSO-S 104A) with a bandwidth of 2.5 GHz and a sampling rate of 20 GSa/s. The Tx signal was used as a trigger for measurements. A bus line was built with a twisted-wire pair with a twist rate of 33 twists/m and an inner conductor size of 0.3 mm2. Its measured characteristic impedance was 121 Ω.

Two types of CAN transceivers were built for testing: a TJA1057 with a 10%–90% fall time of approximately 39 ns and a TJA1040 with that of approximately 9 ns. The effects of stub-line length and the number of stub lines connected to a joint connector were validated using the TJA1057 CAN transceiver supporting data rates up to 5 Mbit/s. The TJA1040 was tested for comparing the effects of transition time on ringing, even though it was a CAN transceiver that did not support CAN-FD operation.

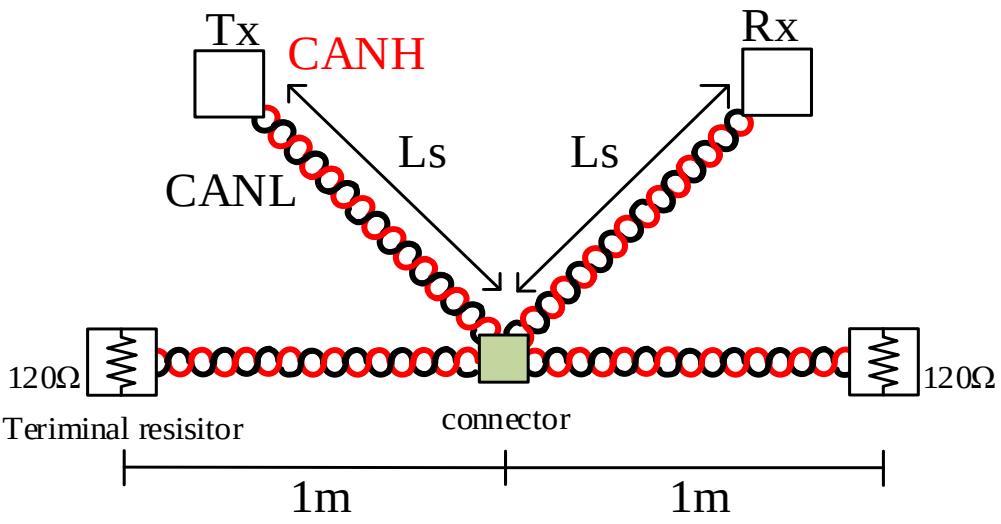

Figure 3.18. The Simulation structure of CAN FD ringing test with Tx and Rx

Table 3.2 the spec of signal timing and Cable length

Normal bit time td	**Valid range for sample point**	**Bus length**	**Max node**
4us	75 ~ 90%	250 m	30
2us	75 ~ 90%	100 m	30
1us	75 ~ 90%	25 m	30
0.5us	75 ~ 90%	-	-
0.4us	75 ~ 90%	-	-
0.2us	75 ~ 90%	10 m	100
0.5us	75 ~ 90%	-	-

B. Simulation result with chip test

Fig. 8 depicts the bus signals measured under different conditions of a dominant-to-recessive transition time. The tested network configuration was as follows: ls = 1 m and n = 2, which were the same as those used for the simulations of Fig. 4. The red solid lines in the left and right panels show the bus signal measured with TJA1040 and TJA1057, respectively.

For comparison, the simulation results were represented by the blue dotted lines and were found to be in accordance with the measurement ones.

From the left panel, the maximum magnitudes of ringing in he measurement and simulation results were 1.37 and 1.41 V, respectively, whose error rate was 2.8%. The ringing periods were 22.5 and 22.4 ns, respectively. The reference time delayed from its first crossing time of 0.5 V were 65 and 87 ns,

respectively. The error rate of the delayed reference time was larger than the other features, but this was because the fourth peak of ringing in the measurement result was 0.45 V, slightly smaller than 0.5 V, while that in the simulation one was 0.58 V, slightly larger than 0.5 V.

The right panel shows that the same network configuration as the left panel maintained the ringing much lower than the threshold level. The magnitudes and ringing periods for the measurement and simulation results were 0.10 and 0.05 V and 28.7 and 26.3 ns, respectively. The simulation result followed well the envelope of the measurement result, even though it showed less clear ringing.

Fig. 9 shows the measured signals for ls = 1 and 2 m in a network configuration of n = 3. TJA1057 was used as the CAN transceiver. The maximum magnitudes of ringing for ls = 1 and 2 m were 0.21 and 0.59 V, respectively, which deviated from the simulation results by 0.01 and −0.04 V. The measured periods for ls = 1 and 2 m were 29.9 and 50.0 ns, respectively, which deviated from the simulation results by 0.0 and 0.5 ns. In the right panel, the delays in the reference times for the measurement and simulation results were 43.5 and 44.4 ns, respectively.

Bit ration 1Mbps	**Bit ration 5Mbps**
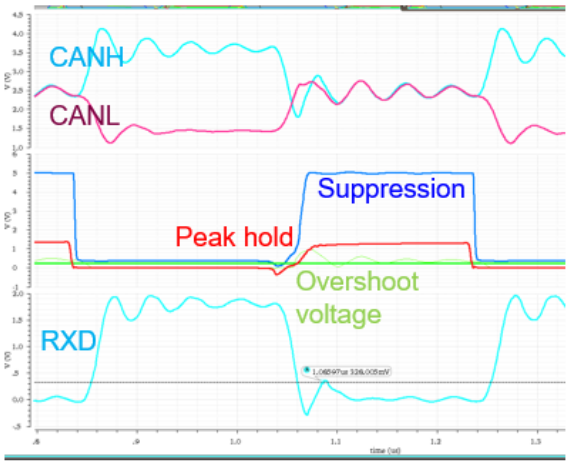	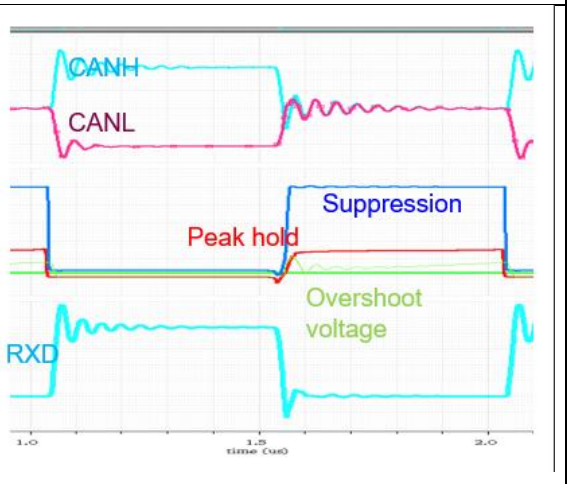

Figure 3.19. The Simulation result of CAN FD at data rate from 1Mbps to 5Mbps

D. Comparison with experimental results

Signal distortion in a physical bus with two connectors is estimated using (22)–(27) and compared with the measurement results in Fig. 12. The considered network configuration is ls = 2 m and n = 3. In each panel, the red solid and blue dotted lines represent the measurement and simulation results, respectively. The black dashed line represents the 0.5-V level, i.e., the threshold level for a recessive state.

.

The other three panels show the physical bus signals for ld = 2, 3, and 5 m. The physical bus signal maintains the form of ringing obtained in the single connector but undergoes a different fluctuation according to the distance between the connectors.

This is because the return signals, which are also a function of the constituent part of ringing, i.e., V1(out), are superposed on ringing but the superposed times are determined by ld and ls. The maximum magnitudes of ringing and the resulting delay in the reference times in physical bus signals are the main causes of the propagation delay asymmetry, which hinders a reliable CAN-FD communication. The simulation and measurement results are compared in Table I. Except for the reference time delay for ld = 5 m, the simulation results are in accordance with the measurement ones at error rates of less than 10%. The relatively large delay for ld = 5 m is because the third peak in the simulation result is 0.53 V, which is slightly larger than 0.5 V.

Table. 3.2 Comparison between simulation and measurement

Voltage		Single connector	LS = 2m	LS = 3m	LS = 5m
Max magnitude	Simulation	0.63V	0.93V	0.82V	0.82V
	Measurement	0.59V	0.85V	0.85V	0.91V
Reference time delay	Simulation	44.4ns	0.93V	0.82V	0.82V
	Measurement	43.5ns	0.85V	0.85V	0.91V

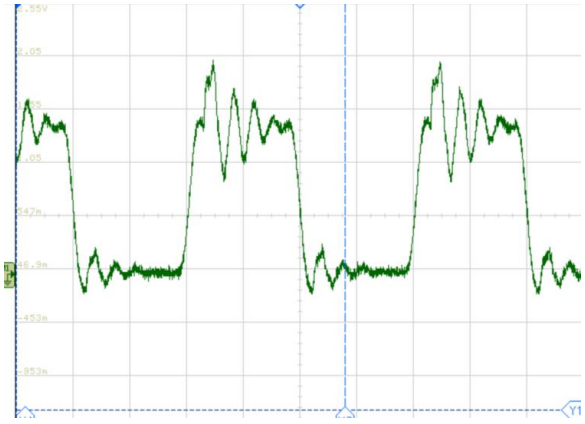

Ls =2 m

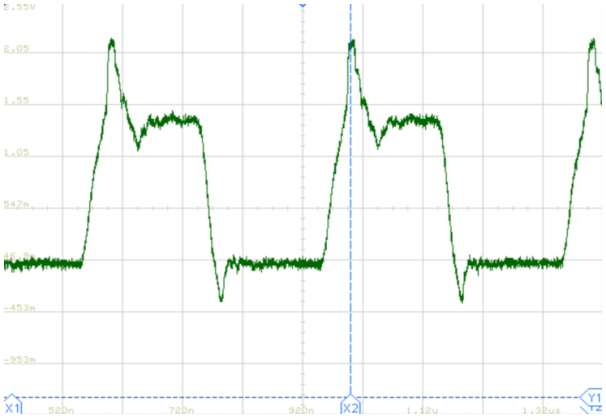

Ls =2 m with ringing suppression

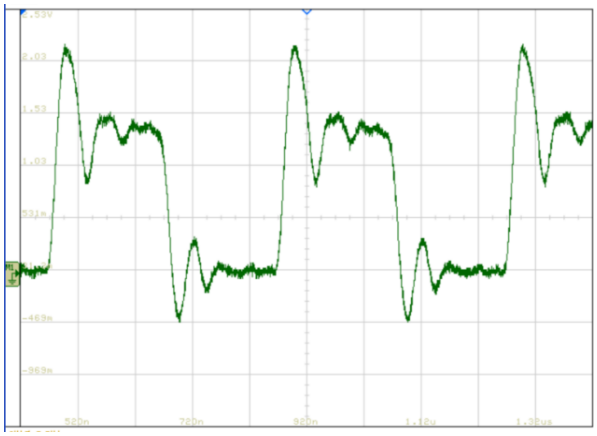

Ls =3 m

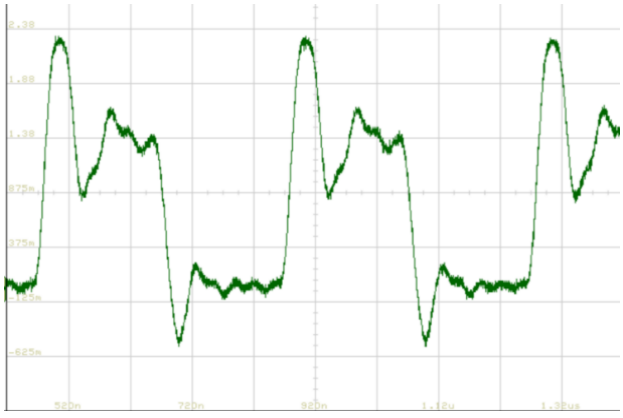

Ls =3 m with ringing suppression

Fig. 3.20. Signals in the physical bus configuration including two connectors

4. Measurement result

4.1 Packaged chip CAN FD with ring suppression method

Fig. 4.1 shows the experimental setup for industrial product, TCAN1041GVDQ1 [3], to compare its performances with the proposed transceiver. This proposed CAN-FD transceivers including proposed method were fabricated using 0.18μm automotive BCDMOS process.

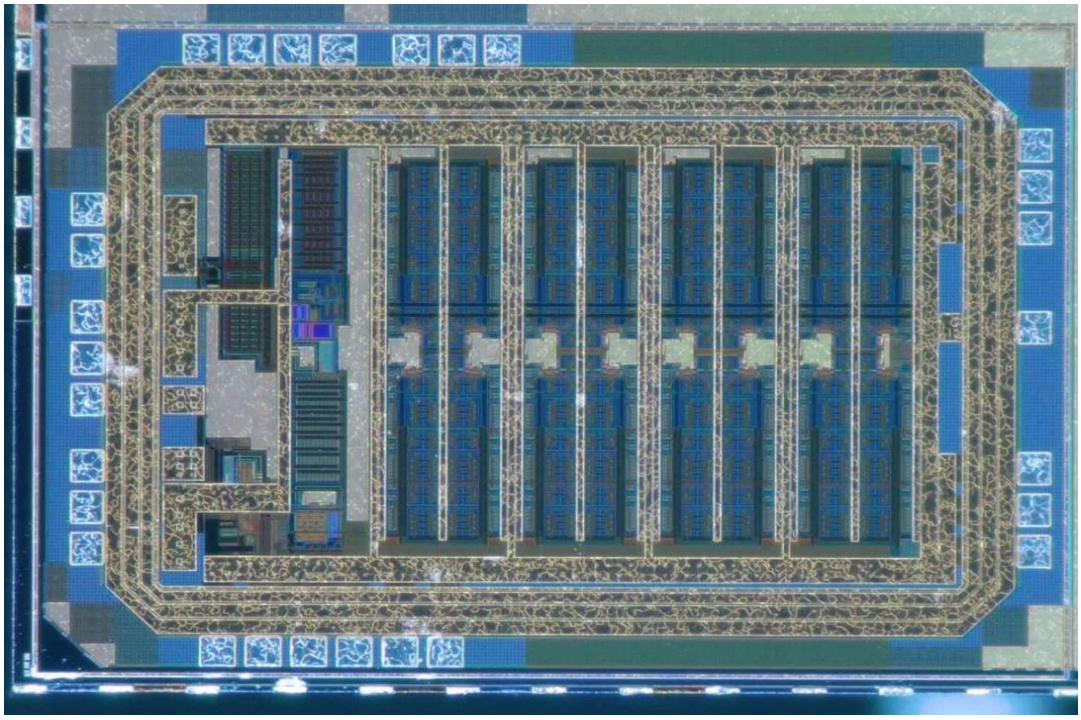

Fig. 4.1. CAN FD IC Chip (TSMC 0.18um)

4.2 Normal operation check of CAN FD

A. Experimental setup- normal operation check

The experimental setup of the proposed CAN-FD transceiver is shown in Fig. 12. Using a power supply, a function generator and an Oscilloscope, an experiment using a single node is performed on the CAN bus. The function generator is used to supply TXD signal which controls the power stage. The power supply supplies 3V and 5V domain powers. The oscilloscope checks the CAN bus and RXD signals. Fig. 4.3 shows the experimental setup for industrial product, to compare its performances with the proposed transceiver. In both set-ups, 30Ω and 60Ω of load resistors (R_L) and 4nF of load capacitors (C_L) are used in the experiments to check the performance of each transceiver. Additionally, 0.1μF of bypass capacitors are connected to a 5V domain power line of both set-ups

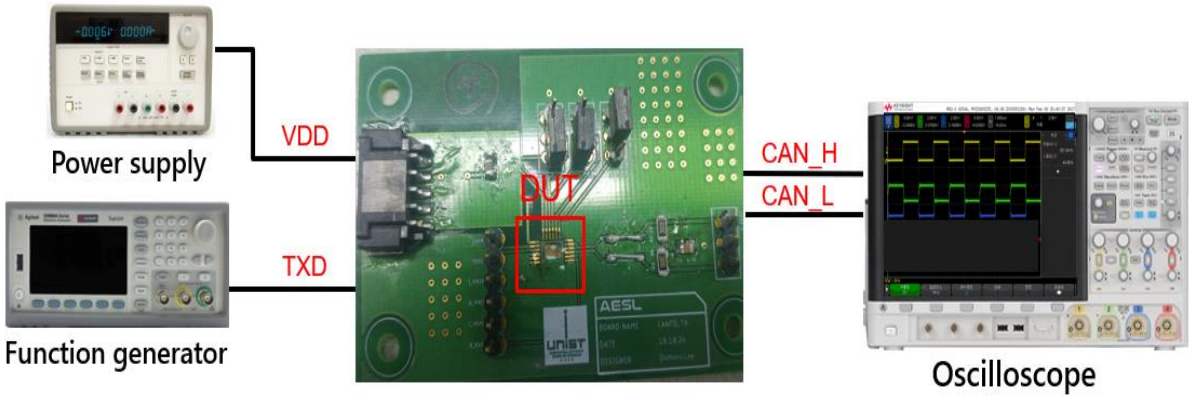

Figure 4.2. Test setup

Table 4.1 Dc characteristic of CAN bus

	SPEC (ISO 11898)			Simulation			TSMC		
	MIN (V)	TYP (V)	MAX (V)	MIN (V)	TYP (V)	MAX (V)	MIN (V)	TYP (V)	MAX (V)
CAN_H	2.75	3.5	4.5	3.24	3.61	3.91	-	3.58	-
CAN_L	0.5	1.5	2.25	1.21	1.43	1.83	-	1.47	-
Vdiff	1.5	2	3	1.41	2.18	2.7	-	2.11	-
Vsym	0.9	1	1.1	-	1.008	-	-	1.01	-

Table 4.2 Switching characteristic

	SPEC (SN65HVD제품 참조)			Simulation			TSMC		
	MIN (ns)	TYP (ns)	MAX (ns)	MIN (ns)	TYP (ns)	MAX (ns)	MIN (ns)	TYP (ns)	MAX (ns)
$t_{d(TXD-BUSon)}$	-	40	70	31.64	35.01	41.64	-	32.57	-
$t_{d(TXD-BUSoff)}$	-	50	70	28.21	36.61	46.49	-	32.25	-
$t_{d(BUSon-RXD)}$	-	70	90	35	37.45	47	-	38.22	-
$t_{d(BUSoff-RXD)}$	-	70	90	34	35.51	58.15	-	39.88	-
$t_{PD(TXD-RXD)}$	-	-	150	68.32	72	93.131	-	71.7	-

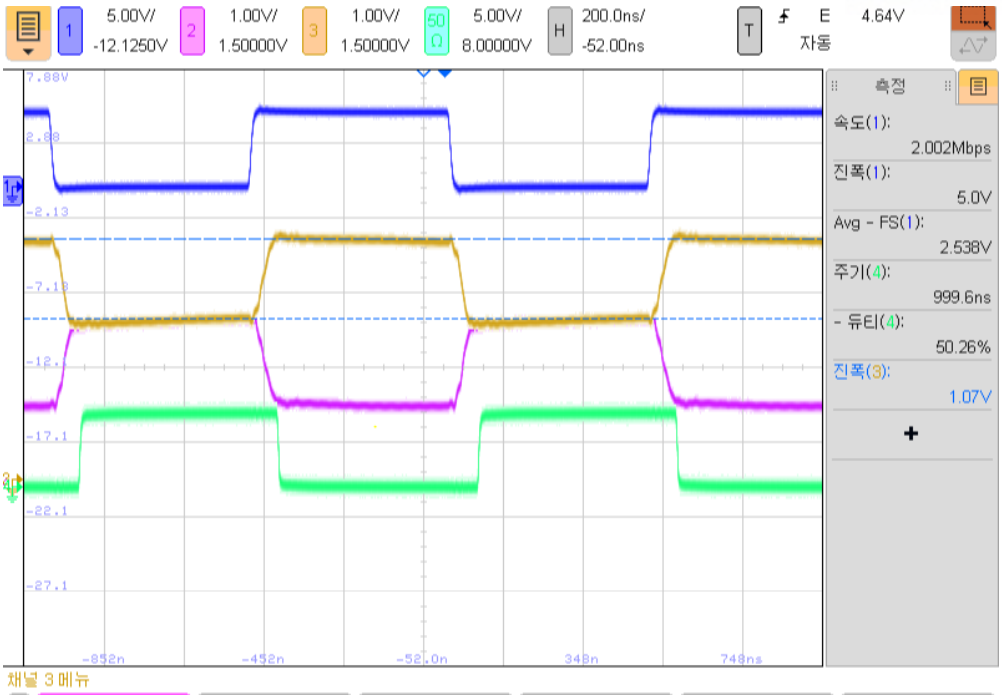

(a)

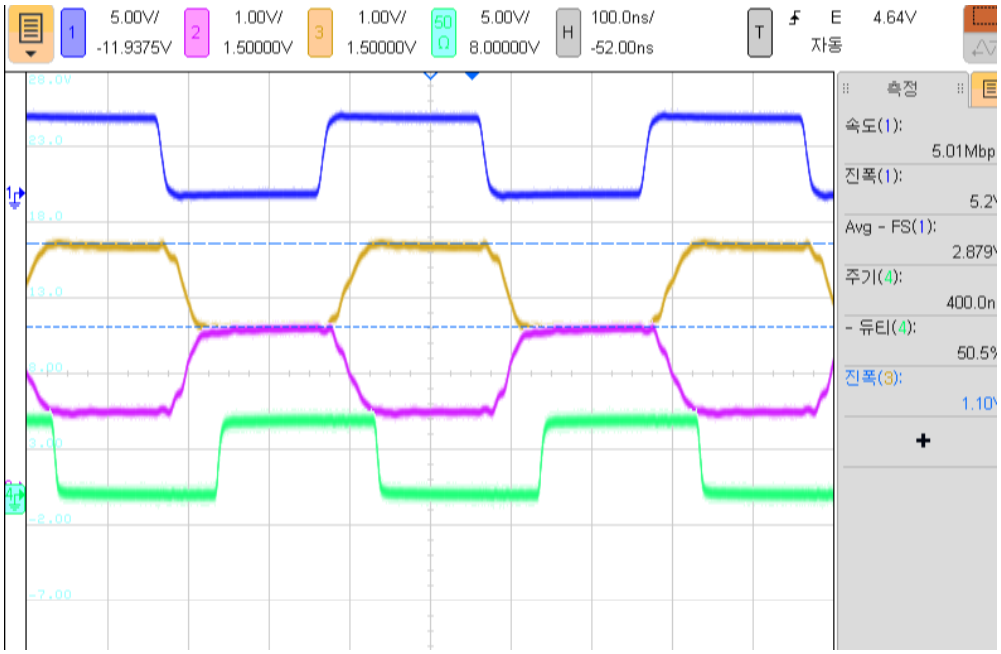

(b)

Fig.4.3 Measurement operation results at 1Mbps (a) 5Mbps (b)

B. ringing suppression experiment

Physical bus signal in transmission for comparison CAN node without ring suppression, i.e.CAN node #1 Circuits were measured using various bus configurations. Created by changing the length and number of stub lines N connected stub lines. Figures 4.2 (a) and (b) show the ringing signal. Measured for ls = 1 m and 2 m respectively in CAN node #1. The green dotted line represents the 0.5 V threshold and Recessive state.

Since a physical bus in a CAN-FD usually included more than one connector, performance of the ringing suppression circuit was tested in a more complex bus configuration with three connectors shown in Fig. 12 (a). The main bus line was 12 m long and each stub line was 1 m long. A total of six CAN nodes were included and two CAN nodes were connected toeach connector. Because more than one connector was inserted, the signalexperienced additional reflections between connectors. Because the connector 2 was directly affected by reflections at connector 1 and 3, CAN node #3 and #4 experienced the most severe ringing. Therefore, CAN node #3 was defined as a transmitter and signals were measured at CAN node #1, #3, #4 and #5.

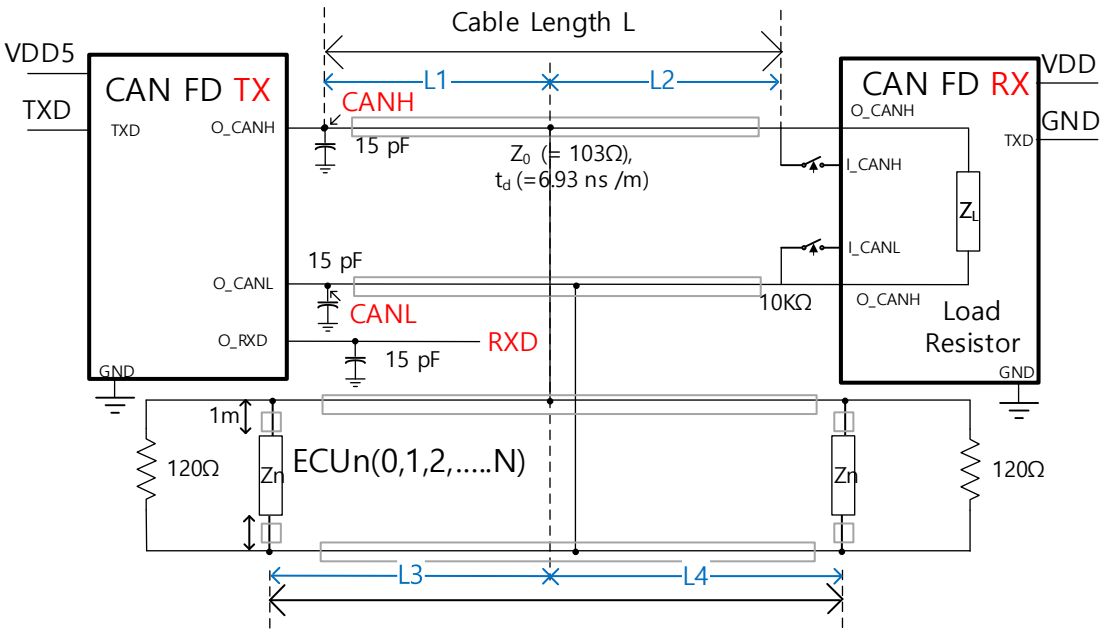

Figure 4.4 (a) the Target setup according to the cable line

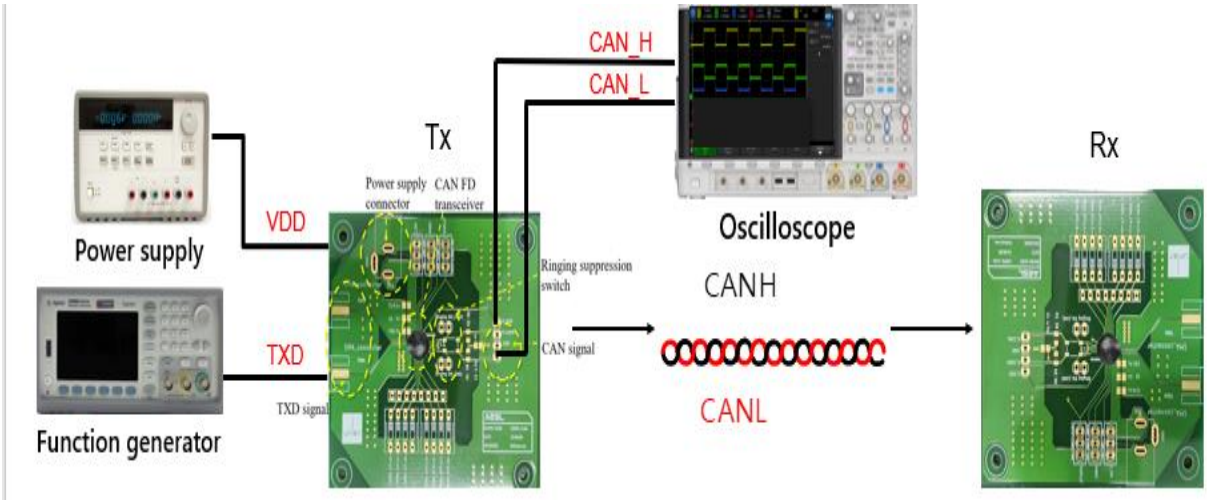

Figure 4.4 (b) the Test setup.

Table. 4.3 Overshoot voltage comparison between ringing and ringing suppression measurement

Bus length	Vpp	Vpp (Suppression Active)	D_{RXD}	D_{RXD} (Suppression Active)
1M	216mV	150 mV	52.6%	51%
2M	258mV	175 mV	52.5 %	51.3%
3M	341 mV	225 mV	53.8 %	51.7 %
4M	508mV	250.5 mV	54.5 %	50.6 %

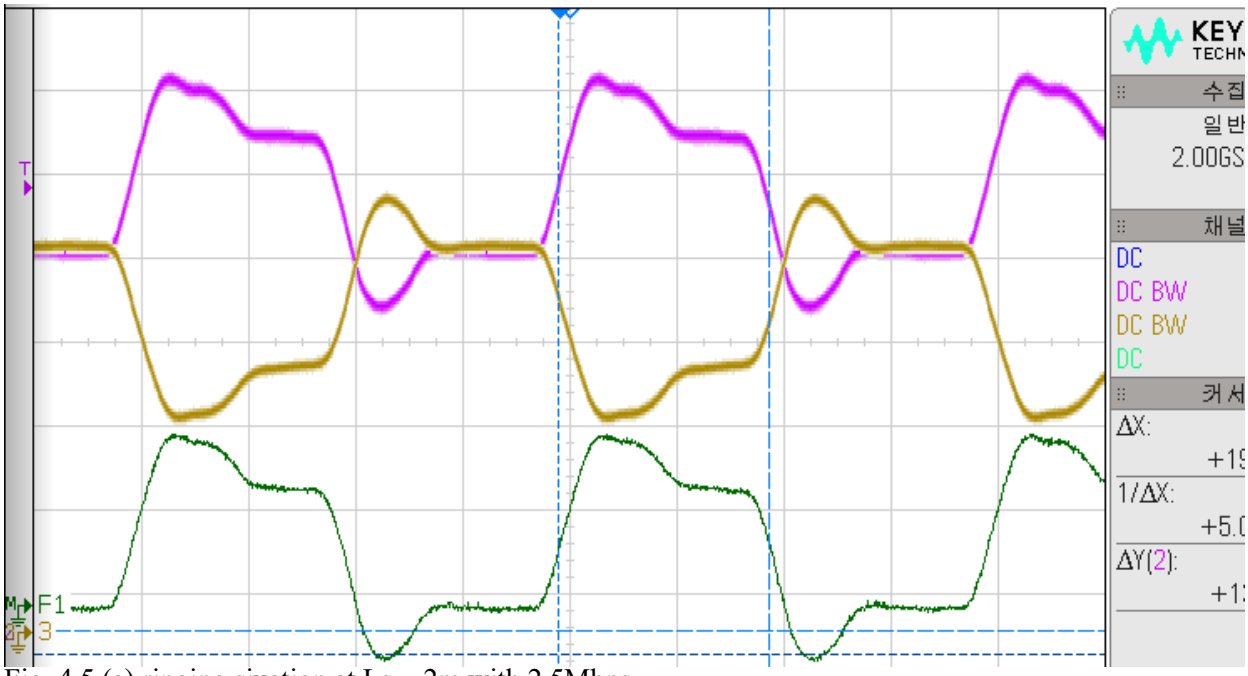

Fig. 4.5 (a) ringing siuation at Ls = 2m with 2.5Mbps

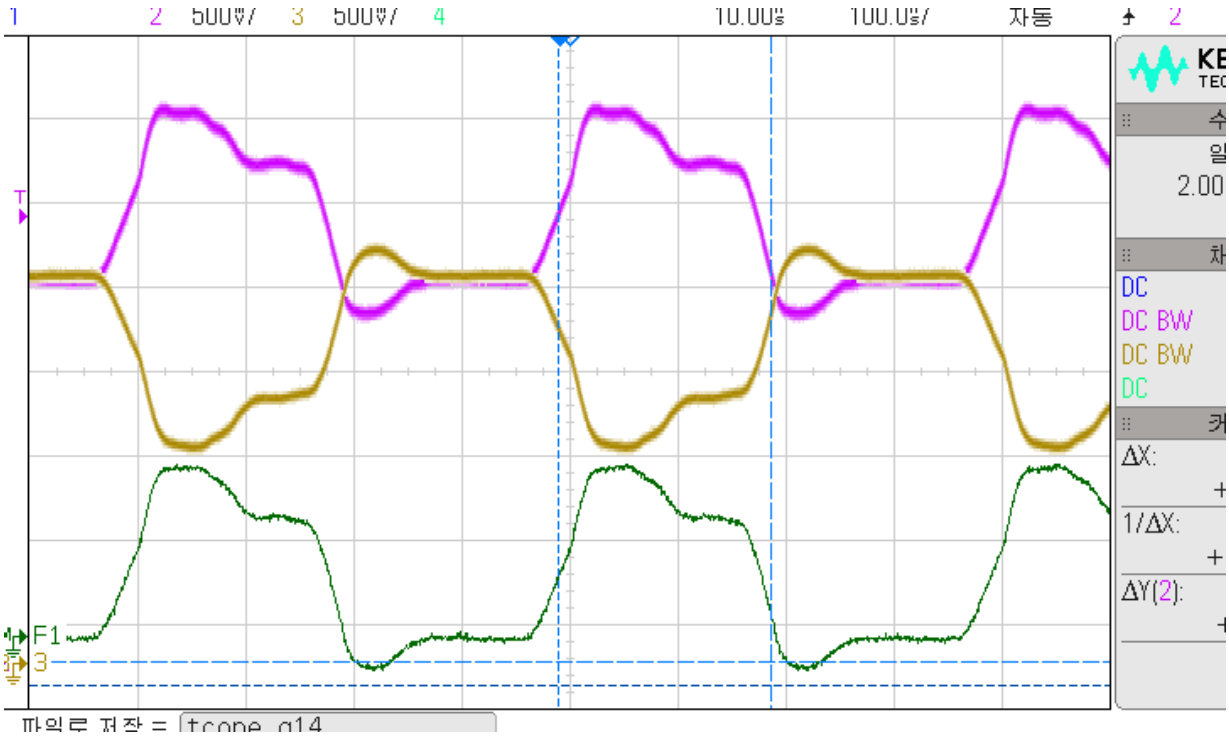

Fig.4.5 (b) ringing suppression actvie at Ls = 2m with 2.5Mbps

5. Conclusion

Ringing is the main cause of asymmetry in the propagation delay and bandwidth degradation of CAN-FD networks. Because ringing is largely dependent on the physical bus configuration, it restricts options for more cost-effective and highly productive physical bus designs.

In this paper, ringing suppression circuits for a CAN-FD were proposed based on analysis of the cause and mechanism of ringing. Then, the performance of the proposed circuits was tested and compared with the signal distortion measured in a normal CAN node without a ringing suppression circuit. The results show that ringing suppression circuits can effectively reduce signal distortion and support more reliable communication in a CAN-FD with a high data rate. Impedance mismatches at the front of a CAN node and the divergence point in here in a physical bus configuration of a CAN-FD. The repeated reflections at the two mismatching points lead to ringing and thus asymmetry in the propagation delay. This ringing primarily occurs during a dominant-to-recessive transition due to inherent characteristics of a CAN transceiver. Therefore, the ringing suppression circuit resolves reflection at the front of the CAN node by temporarily providing impedance matching and/or limiting the maximum magnitude of the ringing.

The ringing suppression circuit was composed of a switch, ringing suppression components, and a switch control circuit. The switch was inserted to allow connection of the ringing suppression components only at the beginning of a recessive state, which is the most probable time of ringing. These components would therefore have no effect on the signal at a dominant state. This switch control was synchronized with the TxD signal of a CAN controller by the switch control circuit.

Three types of ringing suppression components were tested: 1) a 120 Ω resistor for matching the input impedance of the transmitting CAN node with the characteristic impedance of the bus line; 2) a forward-biased diode for limiting the magnitude of signal distortion at the recessive state; and 3) the parallel combination of a resistor and diode for capturing their effects. The experimental results show that all three proposed circuits reduced ringing by more than 50% in comparison with a normal CAN node without a ringing suppression circuit. In particular, the second and third ringing suppression circuits limited ringing at the transmitting node to less than the threshold level of 0.5 V in a CAN bus configuration including a single connector where ls = 2 m and n = 5. Therefore, the proposed ringing suppression circuits can make a signal less dependent on the physical bus configuration, guarantee good symmetry in the propagation delay through an expanded physical bus, and provide reliable CAN-FD communication with a high data rate.

REFERENCES

[1] J. S. Artal, J. Caraballo and R. Dufo, "CAN/LIN-Bus protocol. Implementation of a low-cost serial communication network," 2014 XI Tecnologias Aplicadas a la Ensenanza de la Electronica (Technologies Applied to Electronics Teaching) (TAEE), Bilbao, 2014, pp. 1-8.

[2] ISO 11898: Road Vehicles – Controller Area Network (CAN), International Organization for Standardization, Geneva, Switzerland, 2003.

[3] Texas Instruments Inc., TCAN1042-Q1 Automotive Fault Protected CAN Transceiver with CAN FD, May. 2017.

[4] Atmel, CAN-FD and Ethernet Create Fast Reliable Automotive Data Buses for the Next Decade, 2013.

[5] CAN with Flexible Data-rate, Robert Bosch GmbH, Aug. 2011. [Online] Available at: http://www.semiconductors.bosch.de

[6] CAN in Automation, CAN in Automation (CiA): CAN FD - The basic idea. [Online] Available at: https://www.can-cia.org/can-knowledge/can/can-fd/

[7] Won-Hee Jo, “A CAN Transceiver for a Smart Output ASIC of Automotive Electronic Control Units: Design, Implementation, and Measurement”, 2016.

[8] M. Ramdani, E. Sicard, S. Ben Dhia and J. Catrysse, "Towards an EMC roadmap for Integrated Circuits," 2008 Asia-Pacific Symposium on Electromagnetic Compatibility and 19th International Zurich Symposium on Electromagnetic Compatibility, Singapore, 2008, pp. 8-11.

[9] P. Schröter, M. M. Hell and M. Frey, "EMC compliant LIN transceiver," 2013 Proceedings of the ESSCIRC (ESSCIRC), Bucharest, 2013, pp. 363-366.

[10] J. M. Redoute and M. Steyaert, "An EMI Resisting LIN Driver in 0.35-micron High-Voltage CMOS," in IEEE Journal of Solid-State Circuits, vol. 42, no. 7, pp. 1574-1582, July 2007.

[11] J. m. Redoute and M. Steyaert, "An EMI resisting LIN driver," 2006 Proceedings of the 32nd European Solid-State Circuits Conference, Montreux, 2006, pp. 580-583.

[12] J. M. Redoute and M. Steyaert, "EMI resisting smart-power integrated LIN driver with reduced slope pumping," 2008 IEEE Custom Integrated Circuits Conference, San Jose, CA, 2008, pp. 643-646.

[13] J. G. Janschitz, "An EMI robust LIN driver with low electromagnetic emission," 2015 10th International Workshop on the Electromagnetic Compatibility of Integrated Circuits (EMC Compo), Edinburgh, 2015, pp. 83-86.

[14] A. Gomes, E. P. S. Junior and I. Nascimento, "EMC-EMI Optimized High Speed CAN Line Driver," 2005 18th Symposium on Integrated Circuits and Systems Design, Florianopolis, 2005, pp. 9-14.

[15] M. Gursoy, S. Jahn, B. Deutschmann and G. Pelz, "Methodology to Predict EME Effects in CAN Bus Systems Using VHDL-AMS," in IEEE Transactions on Electromagnetic Compatibility, vol. 50, no. 4, pp. 993-1002, Nov. 2008.

[16] ISO 7637-3:1995 Road Vehicles – Electrical disturbances by conduction and coupling.

[17] D. S. Eddy and D. R. Sparks, “Applications of MEMS technology in automotive sensors and actuators,” Proc. IEEE, vol. 86, no. 8, pp. 1747–1755, Aug. 1998.

[18] S. Franisse, Application Requirements for Smart High-Side Switches, Rev. 1.0, Infineon Technologies AG., Dec. 2010. [Online]: https://www.infineon.com

[19] BOSCH—CAN Specification Version 2.0, (1991). [Online]. Available: http://www.bosch.com

[20] W. Prodanov, M. Valle and R. Buzas, "A Controller Area Network Bus Transceiver Behavioral Model for Network Design and Simulation," in IEEE Transactions on Industrial Electronics, vol. 56, no. 9, pp. 3762-3771, Sept. 2009.

[21] CAN in Automation, CiA 601 Part 1: Physical interface implementation Version 2.0.0, Feb. 2017.

[22] M. Deloge, A. van der Wel, S. Goyal, G. Kwakernaat and A. Schoof, "A highly-digitized automotive CAN transceiver in 0.14 µm high-voltage SOI CMOS," 2015 10th International Workshop on the Electromagnetic Compatibility of Integrated Circuits (EMC Compo), Edinburgh, 2015, pp. 13-17.

[23] P. L. Hower and S. Merchant, "Snapback and safe operating area of LDMOS transistors," International Electron Devices Meeting 1999. Technical Digest (Cat. No.99CH36318), Washington, DC, USA, 1999, pp. 193-196.

[24] W. L. Terçariol, R. L. T. Saez and I. C. R. Nascimento, "High and low side high voltage switch with over voltage and over current protection," 2013 IEEE Computer Society Annual Symposium on VLSI (ISVLSI), Natal, 2013, pp. 177-181.

[25] EMC Evaluation of CAN Transceivers, 47A/747/DTS. IEC/TS 62228, February 2007.

[26] Integrated Circuits - Measurement of Electromagnetic Emissions - 150kHz to 1GHz - Part 4: Measurement of Conducted Emissions - 1Ω /150Ω Direct Coupling Method. IEC 619677-4, 2006.

[27] Integrated Circuits - Measurement of Electromagnetic Immunity - 150kHz to 1GHz - Part 4: Direct RF Power Injection Method. IEC 62132-4, 2006.

[28] H. Mori, N. Maeda, Y. Mori, H. Obata, Y. Kaku and S. Akasaki, "Novel ringing suppression circuit to achieve higher data rates in a linear passive star CAN FD," 2014 International Symposium on Electromagnetic Compatibility, Gothenburg, 2014, pp. 402-407.

[29] CAN in Automation, CiA 601 Part 4: Physical interface implementation Version 2.0.0, Feb. 2017.